The Common Representative Intermediates Mechanism version 2 in the United Kingdom Chemistry and Aerosols Model

S. Archer-Nicholls[1], N. L. Abraham[1,2], Y. M. Shin[1], J. Weber[1], M. R. Russo[1,2], D. Lowe[3], S. Utembe[4], F. M. O'Connor[5], B. Kerridge[6,7], B. Latter[6,7], R. Siddans[6,7], M. Jenkin[8], O. Wild[9], A. T. Archibald[1,2]

[1]Department of Chemistry, University of Cambridge, Cambridge, UK
[2]National Centre for Atmospheric Science, Department of Chemistry, University of Cambridge, Cambridge, UK
[3]University of Manchester, Manchester, UK
[4]University of Melbourne, Melbourne, Australia
[5]Met Office Hadley Centre, Exeter, UK
[6]Remote Sensing Group, STFC Rutherford Appleton Laboratory, UK
[7]NERC National Centre for Earth Observation, Rutherford Appleton Laboratory, UK
[8]Atmospheric Chemistry Services, Okehampton, Devon, UK
[9]Lancaster University, Lancaster, UK

Key Points:

- The CRI-Strat mechanism has been integrated into the UKCA model, greatly increasing the complexity of VOC chemistry compared to StratTrop.
- CRI-Strat simulates higher surface ozone compared to StratTrop due to greater production, but tropospheric ozone burden is similar.
- The ozone and oxidised nitrogen budgets when running with the CRI-Strat mechanism show high sensitivity to the input NMVOC emissions.

Corresponding author: Alex T. Archibald, `ata27@cam.ac.uk`

Abstract

We document the implementation of the Common Representative Intermediates Mechanism version 2, reduction 5 (CRIv2-R5) into the United Kingdom Chemistry and Aerosol model (UKCA) version 10.9. The mechanism is merged with the stratospheric chemistry already used by the StratTrop mechanism, as used in UKCA and the UK Earth System Model (UKESM1), to create a new CRI-Strat mechanism. CRI-Strat simulates a more comprehensive treatment of non-methane volatile organic compounds (NMVOCs) and provides traceability with the Master Chemical Mechanism (MCM). In total, CRI-Strat simulates the chemistry of 233 species competing in 613 reactions (compared to 87 species and 305 reactions in the existing StratTrop mechanism). However, while more than twice as complex than StratTrop, the new mechanism is only 75% more computationally expensive. CRI-Strat is evaluated against an array of *in situ* and remote sensing observations and simulations using the StratTrop mechanism in the UKCA model. It is found to increase production of ozone near the surface, leading to higher ozone concentrations compared to surface observations. However, ozone loss is also greater in CRI-Strat, leading to less ozone away from emission sources and a similar tropospheric ozone burden compared to StratTrop. CRI-Strat also produces more carbon monoxide than StratTrop, particularly downwind of biogenic VOC emission sources, but has lower burdens of nitrogen oxides as more is converted into reservoir species. The changes to tropospheric ozone and nitrogen budgets are sensitive to the treatment of NMVOC emissions, highlighting the need to reduce uncertainty in these emissions to improve representation of tropospheric chemical composition.

Plain Language Summary

To understand the climate and predict how it will change in the future, we need to understand its chemical composition - the trace gases and small particles that exist in tiny quantities in the atmosphere. A key tool we use to do this are computer models which simulate the atmosphere and processes within it. Key processes include the formation of ozone, a harmful pollutant and greenhouse gas in the lower atmosphere. However, the chemistry involved in forming ozone is very complicated, so computer simulations of the atmosphere must greatly simplify the chemistry. These simple schemes may introduce errors in the model. We also have much more complex chemical mechanisms which simulate our best understanding of all chemical reactions, but these complex schemes require too much computational power to be used when simulating the whole atmosphere. In this paper, we describe the implementation of a chemical mechanism that sits between these levels of complexity, realistically simulating the formation and destruction of ozone without being too slow to run. We compare this new mechanism against measurements taken of the atmosphere and the preexisting, simpler chemical mechanism and show that the new mechanism greatly enhances the amount of ozone that is produced.

1 Introduction

Understanding chemical processes in the lower atmosphere is of vital importance for tackling the problems of air pollution and making accurate projections of how the Earth system will change due to human activity (Sillman, 1999; Akimoto, 2003; Von Schneidemesser et al., 2015; Monks et al., 2015; Boucher et al., 2013). However, the chemistry of the troposphere is extremely complicated because of the wide variety of non methane volatile organic compounds (NMVOCs) whose structures are diverse and whose lifetimes and abundances cover many orders of magnitude (Atkinson, 1990; M. Jenkin et al., 1997; Goldstein & Galbally, 2007). Two particularly challenging aspects of tropospheric chemistry regard the understanding of the formation and destruction of tropospheric ozone and the impacts of aerosols, with much of the difficulty in both of these research topics stemming from the importance of NMVOCs. The rate of production of ozone is non-

linearly dependent on the combination of nitrogen oxides ($NO_x = NO \cdot NO_2$) and NMVOCs levels, with high rates of ozone production occurring when levels of both are high and net ozone destruction occurring when there is a large excess of NMVOCs (NO_x-limited regime) or an excess of NO_x (VOC-limited regime) (Sillman, 1999; Monks et al., 2015). Larger NMVOC molecules, such as monoterpenes, aromatic compounds and long chain n-alkanes ($C_{>10}$ – where C indicates the number of carbon atoms in the NMVOC) play an important role in the generation of secondary organic aerosol (SOA). SOA can make up over 50% of submicron aerosol mass (Jimenez et al., 2009), but we still have significant uncertainty in the exact chemical makeup, and models still fail to accurately simulate it (Tsigaridis et al., 2014; Hodzic et al., 2020). Unfortunately, many thousands of different NMVOC species have been identified in the atmosphere, and many more are yet to be discovered, making a complete representation of all NMVOC species and their chemistry in a model an impossible task (Goldstein & Galbally, 2007; Heald & Kroll, 2020).

The key mapping between the input NMVOCs and their effects on ozone and SOA is their oxidation mechanism. Such mechanisms are well known from laboratory experiments for the simplest NMVOCs ($C_{<5}$). Based on the wealth of experimental data (McGillen et al., 2020), structure activity relationships (SARs) have been derived to fill in the gaps (M. E. Jenkin et al., 2018b, 2018a; M. E. Jenkin, Valorso, et al., 2019) and to extrapolate our understanding of NMVOC oxidation to cover a wide range of structures and configurations. Aumont et al. (2005) have shown that the oxidation process in the atmosphere can be treated as a geometric problem, with the number of species produced during the oxidation of an alkane NMVOC with n carbon atoms being given by:

$$\Omega \approx \sum_{i=2}^{n} \frac{1}{2} (11)^2 (7)^{i-2} . \tag{1}$$

For a C_5 compound, this equation leads to $\approx 10^5$ species forming, presenting a huge amount of complexity.

To approach the problems of complexity relating to NMVOC chemistry in the atmosphere, researchers have typically followed one of two routes for developing chemistry mechanisms depending on the research questions being tackled and relevant spatial and temporal scales. Detailed, explicit mechanisms (Aumont et al., 2005) and near-explicit mechanisms, such as the Master Chemical Mechanism (MCM; Saunders et al. (2003); M. E. Jenkin et al. (2003)), comprise of the amalgamation of known relevant chemistry as measured from laboratory chemical kinetic studies (Atkinson et al., 2006; S. P. Sander et al., 2011) and SARs (M. E. Jenkin et al., 2018b, 2018a; M. E. Jenkin, Valorso, et al., 2019) and evaluated against field and chamber experiments (M. E. Jenkin et al., 2012; Novelli et al., 2018). These mechanisms represent our best understanding of chemical processes in the atmosphere, often comprising of thousands of species and many times more reactions, and are continuously updated and expanded as new data and understanding comes to light. However, this makes them computationally very expensive to run and hence these explicit mechanisms are mostly used in box model studies (M. E. Jenkin et al., 2015; Derwent, 2017).

An alternative design approach is to construct mechanisms that are as simple as possible but as complicated as necessary, the aim being to represent the key chemical processes and their interactions with as few chemical species and reactions as possible. Such atmospheric chemistry schemes typically have 10s of species and dozens to hundreds of reactions (e.g., the StratTrop scheme which simulates 81 species, 291 reactions (Archibald et al., 2020)). Chemical processes are still informed by the best available data, but similar species are lumped together or represented by surrogate species and more complex but important processes are parameterised to reduce the mechanism complexity. Mechanisms may also become quite specialist, with those designed to simulate urban air pollution (e.g., (Stockwell et al., 1990)) differing greatly from those intended to simulate the whole atmosphere at a coarse resolution (e.g., (Archibald et al., 2020)), as

they focus on different aspects of the chemistry system occurring in the real atmosphere. These approximations are necessary to run interactive chemistry in 3D models that must also simulate other key processes such as transport, deposition, clouds and radiation. Even so, the chemistry component is often the most computationally expensive part of a 3D model (Esenturk et al., 2018).

These different approaches leave open a gap between our most comprehensive mechanisms and simpler ones. Simpler schemes can perform well for the photochemical conditions they were designed for, but may perform poorly when simulating other regions, or fail to properly represent how chemical conditions should change in response to changes in emissions or climate. Due to their complexity, it is impractical to use near-explicit chemistry schemes in the same 3D model setup as simpler mechanisms to see how they would perform instead. While they can be evaluated against comprehensive schemes in box model simulations, when results differ it is difficult to pinpoint which aspect of the chemistry is causing the differences, due to the lack of traceability, and it can be unclear whether the simpler mechanisms respond realistically in photochemical conditions outside of those evaluated in box model experiments. There is therefore a clear need for intermediate complexity mechanisms - ones which are fully traceable to more comprehensive schemes and are known to respond similarly to changes in forcings, but are still simple enough to be used in 3D interactive models.

The Common Representative Intermediates (CRI) mechanism (M. E. Jenkin et al., 2002; M. Jenkin et al., 2008) is just such an intermediate complexity mechanism. The number of species and reactions are reduced by over an order of magnitude compared with the MCM. However, through a rigorous development process, in which it was fully and systematically evaluated against the more complex MCM mechanism at each stage of complexity reduction and no change that significantly degraded representation of ozone production was allowed through (Watson et al., 2008), the scheme is fully traceable to the MCM. The end result is a mechanism that is simple enough to be run in a 3D model, but which we can be confident responds to changes in emissions and conditions according to our best understanding as represented in the MCM. Intermediate complexity mechanisms offer enormous benefits when used in 3D models as a research tool to study the importance of chemical processes which are ignored in simpler schemes and as a benchmark against which to test, evaluate and inform development of these simpler schemes. By having more confidence in the representation of gas-phase chemistry, it is possible to attribute remaining model biases to other structural components of the model.

The CRI mechanism has been used in several models now, including the STOCHEM Lagrangian global chemical transport model (S. Utembe et al., 2010; M. A. H. Khan et al., 2015), the Weather Research and Forecasting model with chemistry (WRF-Chem), an online regional coupled model (Archer-Nicholls et al., 2014; Lowe et al., 2015; M. A. Khan et al., 2019) and in a regional nested configuration of the European Monitoring and Evaluation Programme chemical transport model for the UK (EMEP4UK) (Hood et al., 2018). However, to the best of our knowledge, it has never been used in a global chemistry-climate model. In this paper we document the implementation of the CRIv2-R5 mechanism in the United Kingdom Chemistry and Aerosol (UKCA) model (Morgenstern et al., 2009; O'Connor et al., 2014), as used in the Met Office Unified Model (UM) and the UK's Earth System Model (UKESM1) (Sellar et al., 2019), evaluate it against a suite of observations and rigorously compare the new mechanism to the existing chemical mechanism (Strat-Trop; Archibald et al. (2020)). We note that there are differences in the reaction rate coefficients in the two mechanisms that reflect their independent development and reliance on different assessments of kinetic parameters, which has a bearing on model simulations (Newsome & Evans, 2017). We also explore how differences in the allocation of NMVOC emissions in the two mechanisms contributes to the differences between them.

The UKESM1 model is used for quantifying and understanding climate forcing, including as part of the Coupled Model Intercomparison Project Phase 6 (CMIP6) (Eyring

et al., 2016), making projections of future air quality (including crop yields and human health impacts), and increasingly being used to quantify impacts of mitigation. The implementation of the CRI mechanism into the UKCA, UM and UKESM1 models represents a step change the potential for simulating the complex chemistry-climate interactions between ozone and NMVOCs in the coupled Earth System across many chemical environments and multi-century timescales.

2 Model Description

2.1 The UKCA model

The United Kingdom Chemistry and Aerosols (UKCA) model is a sub-model of the Met Office Unified Model (UM) and is designed to simulate atmospheric composition for weather and climate modelling. UKCA is a part of the UKESM1 (Sellar et al., 2019) Earth system model, and uses the Chemistry of Stratosphere and Troposphere (Strat-Trop) chemical mechanism (Archibald et al., 2020), which merges the Stratospheric and Tropospheric chemical mechanisms described by (Morgenstern et al., 2009) and (O'Connor et al., 2014), respectively. The UKCA model provides ozone, methane, and nitrous oxide fields to the UM radiation scheme, as well as calculating oxidant fields that are used to drive the GLOMAP-mode aerosol scheme (Mann et al., 2010; Mulcahy et al., 2018, 2020).

The StratTrop chemical mechanism and its implementation in UKESM1 is described in detail by Archibald et al. (2020). It uses the Fast-JX photolysis scheme (Neu et al., 2007), which was implemented in UKCA as described by Telford et al. (2013). The ASAD chemical mechanism framework (Carver et al., 1997) is used to provide a flexible and extendable approach to mechanism development and to enable a choice of numerical integration schemes. A sparse-matrix Newton-Raphson chemical solver (Wild & Prather, 2000) is used here, applying the quasi-Newton approximations recommended by Esenturk et al. (2018) to reduce run time. Wet deposition of soluble chemical compounds is parameterised following Giannakopoulos et al. (1999) and dry deposition is based on the resistance type model of Wesley (1989), as described by O'Connor et al. (2014).

2.2 The Common Representative Intermediates Mechanism

The Common Representative Intermediates (CRI) Mechanism has been described in detail in previous papers (M. E. Jenkin et al., 2002; M. Jenkin et al., 2008; Watson et al., 2008; S. R. Utembe et al., 2009), so this section only covers a brief overview of the design philosophy. CRI is a fully traceable, reduced complexity representation of the Master Chemical Mechanism (MCM) (M. E. Jenkin et al., 2002; Saunders et al., 2003), with CRI version 2 optimised against the MCM version 3.1. The chemistry of inorganic compounds and smaller initial organic molecules (such as methane, ethane and ethene) is functionally identical in CRI to the full MCM. However, the CRI scheme substantially reduces the total number of species and reactions by lumping the intermediate oxidation products of larger NMVOC species based on an index defined as the total number of carbon-carbon $(C-C)$ and carbon-hydrogen $(C-H)$ bonds, counting double bonds $(C=C)$ as two. This "CRI index" can be understood as the maximum potential number of O_x molecules $(O_x = O_3 + NO_2)$ generated by the VOC in question, assuming complete oxidation to CO_2 and H_2O, with every HO_2 and RO_2 molecule created converting one NO molecule to NO_2, thereby generating one ozone molecule when the NO_2 is photolysed (M. E. Jenkin et al., 2002). This means that every primary NMVOC species in CRI will produce the same number of ozone molecules as its equivalent in the MCM, even though the mechanism is greatly simplified by lumping together similar intermediate species. The intermediate species are named according to their structure, CRI index and functional group as explained in the supplementary Table S1. Using this lumping method, the number of species and reactions in the CRIv2 mechanism is reduced to

434 species and 1183 reactions from 4500 species and $\approx$12600 reactions in MCMv3.1, covering the degradation of the same 115 emitted NMVOC species without compromising the mechanism's ability to simulate ozone production.

The CRIv2 scheme also underwent several further stages of complexity reduction by lumping together emitted species, with the reduced mechanisms evaluated against the MCM at each stage to preserve ozone forming potential, as described by Watson et al. (2008). The version implemented in the UKCA model is the simplest of these reductions, reduction number five (CRIv2-R5) with 196 species, the same version as implemented into the WRF-Chem model (Archer-Nicholls et al., 2014) and STOCHEM-CRI model (S. Utembe et al., 2010; M. A. H. Khan et al., 2015). This version includes the full CRIv2 degradation of isoprene, α-pinene, β-pinene and several aromatic species known to contribute to secondary organic aerosol (SOA) production, as described by S. R. Utembe et al. (2009).

3 Implementation of CRIv2-R5 in UKCA

The CRIv2-R5 chemical mechanism was designed for use in boundary layer/urban air quality scenarios. Compared to the StratTrop mechanism used in UKCA, it represents the chemistry of the following primary NMVOCs and their products which either do not exist or are heavily parameterised in StratTrop:

1. C4 alkane chemistry via n-butane (C4H10)
2. C2-C4 alkene chemistry via ethene, propene and trans-2-butene (C2H4, C3H6 and TBUT2ENE).
3. Alkyne chemistry via C2H2.
4. Expanded biogenic volatile organic compound (BVOC) chemistry with explicit isoprene (C5H8) degradation and additional monoterpene chemistry via α-pinene and β-pinene (APINENE and BPINENE).
5. Aromatic chemistry via benzene, toluene and o-xylene (BENZENE, TOLUENE and OXYLENE).
6. Higher oxidised NMVOC chemistry with the addition of Ethanol (EtOH), propanal (EtCHO) and methyl ethyl ketone (MEK).

In addition, it expands on several key chemical processes, for example all peroxy radicals (RO_2) can react with all other peroxy radicals ($RO_2 + R'O_2$) and most can form organonitrates from $RO_2 + NO$ reactions. However, CRIv2-R5 lacks key photolysis reactions and chemical species which are important for the chemistry of the upper atmosphere. The UKCA chemistry-aerosol model is designed to be used in the UK Met Office Unified Model (UM) and UK Earth System Model (UKESM1) configurations (Sellar et al., 2019), which simulate the whole atmosphere up to a model top of 85 km in the lower mesosphere. Hence, some changes were made to make the CRIv2-R5 scheme suitable for simulating stratospheric chemical conditions as well as the troposphere. In all, the following development tasks were made to import the CRIv2-R5 mechanism into the UKCA model such that it was suitable for use in a 3D Earth System model configuration:

1. Capability for peroxy radical self- and cross-reactions with summed RO_2 pool.
2. Adding stratospheric chemistry, using the same species and reactions as used in the StratTrop mechanism.
3. Coupling with the GLOMAP aerosol mechanism.
4. Linking with online Fast-JX photolysis.
5. Wet and dry deposition of species added.

Table 1. Comparison of gas-phase chemical mechanisms: the StratTrop chemical mechanism as described by (Archibald et al., 2020); the CRIv2-R5 mechanism used as the basis of development as described by M. Jenkin et al. (2008); Watson et al. (2008); S. R. Utembe et al. (2009); CRI-Strat which is CRIv2-R5 combined with species and reactions needed for simulating the stratosphere taken from the StratTrop mechanism; and CRI-Strat+GLOMAP-mode which further includes species and reactions needed for aerosol production.

	StratTrop + GLOMAP-mode	CRI-v2-R5	CRI-Strat	CRI-Strat + GLOMAP-mode
No. Species	87	198	219	233
No. Tracers	83	146	167	181
No. Non transported prognostics	4	52	52	52
No. Peroxy radicals*	9	47	47	47
No. Emitted species	23	27	27	38
No. Photolysis reactions	60	100	124	128
No. Bimolecular reactions	212	451	536	554
No. Termolecular reactions	25	29	36	39
No. Heterogeneous reactions	8	0	5	8
No. Wet deposited species	34	74	80	83
No. Dry deposited species	41	124	128	131

* Peroxy radicals are transported tracers in the StratTrop mechanism,

Table 1 gives a summary of the chemical mechanisms as integrated into the UKCA model, with the CRI-Strat mechanism with coupling to GLOMAP-mode aerosol being the full mechanism described and analysed in this paper. The CRI-Strat mechanism was implemented into UKCA using the ASAD framework (Carver et al., 1997), meaning it can now easily be ported to other models which share the same framework such as TOM-CAT/SLIMCAT chemical transport model (CTM) (Chipperfield, 2006), the offline GLObal Model of Aerosol Processes (GLOMAP) (Spracklen et al., 2006) or the Frontier Research System for Global Change (FRSGC) version of the University of California, Irvine (UCI) global CTM(CTM) (Wild et al., 2000). The full CRI-Strat+GLOMAP-mode mechanism has over twice the number of species (83 to 181) and reactions (305 to 729) as the Strat-Trop mechanism. However, the run time is only about 75% longer, hence achieving a greater than doubling of complexity for less than double the cost (details in Section S1 of the supplement). While still computationally expensive and not designed to replace Strat-Trop for all model studies, multi-century Earth System model simulations with the mechanism are plausible.

The CRIv2-R5 mechanism used to build CRI-Strat was originally optimised against the MCMv3.1 (M. E. Jenkin et al., 2003; Saunders et al., 2003), which drew heavily on kinetic parameters evaluated by the International Union of Pure and Applied Chemistry (IUPAC) Task Group on Atmospheric Chemical Kinetic Data Evaluation (e.g., Atkinson et al. (1997, 2004)). In contrast, the StratTrop scheme (Archibald et al., 2020) draws on a mixture of data from the MCMv3.2 website, the IUPAC Task Group web pages and the NASA JPL Evaluation No. 17 (S. P. Sander et al., 2011). The reaction rate coefficients for common reactions therefore do not always agree, including for some reactions which are extremely important for tropospheric composition. In some cases CRI-Strat is out of date, in others the mechanisms are simply different as they have different sources. Key differences in rate coefficients are documented in Section S4 of the supplement. The CRI version 2.2 mechanism was recently released (M. E. Jenkin, Khan, et al., 2019) and, among other developments, had some of its reaction rates coefficients revised to match

recent assessments to be consistent with MCMv3.3.1 (M. E. Jenkin et al., 2015). Unfortunately, this release was too late to be integrated into the development cycle for the mechanism presented in this paper. However, updating the mechanism to CRI version 2.2 is part of ongoing work.

The remainder of this section describes the developments and implementation of the CRI-Strat mechanism in detail.

3.1 Peroxy Radical Chemistry

Peroxy radicals (RO_2), a class of short-lived compounds formed during oxidation of VOCs, play a crucial role in the formation of tropospheric ozone (Lightfoot et al., 1992) and secondary organic aerosols (Bianchi et al., 2019; Mcfiggans et al., 2019). While in high-NOx environments they tend to react with NO, forming NO_2 and ozone (M. Jenkin & Clemitshaw, 2000; Monks, 2005), in low-NO_x environments they usually react either with HO2 to form hydroperoxides (ROOH), themselves (self-reactions) or other RO_2 species (cross-reactions) (Tyndall et al., 2001; Orlando & Tyndall, 2012). However, because individually simulating the reaction of each RO_2 species with every other RO_2 species for the 47 RO_2 species in CRIv2-R5 would be prohibitively expensive, the approximation described by M. Jenkin et al. (1997) is used, whereby each peroxy radical undergoes a reaction with the summed total of all peroxy radical species (the "RO_2 pool"). The second order reaction rate coefficient is calculated as the geometric mean of the self-reaction rate of the peroxy radical species in question and the $CH_3O_2 + CH_3O_2$ reaction rate. The RO_2 pool is not consumed by these reactions, hence these RO_2-permutation reactions can be thought of as pseudo-unimolecular reactions with a first order rate coefficient proportional to the total RO_2 concentration.

To enable this chemistry within the framework of the UKCA model, peroxy radicals were defined as a unique type - that of a non transported prognostic field. Within the ASAD framework and chemical solver, peroxy radicals are treated like other chemical tracers, but in the rest of the model they are not transported as this is unnecessary for such short lived species. Avoiding the transportation of the 47 peroxy radical species offers substantial savings as some of the largest computational costs of the UKCA model come from tracer transport (Esenturk et al., 2018). The definition of peroxy radicals as a unique type also provides a simple method of tagging the species for their concentrations to be summed when calculating the total RO_2 pool. The RO_2 pool is defined as a field that can affect the rates of reactions but does not have its concentration directly changed from chemical reactions. Instead, its concentration is calculated for each gridcell and is updated as the concentrations of constituent RO_2 species change. Because ASAD uses an implicit backward euler solver with Newton Raphson iteration (Carver et al., 1997; Wild et al., 2000), the RO_2 pool is recalculated with each iteration of the solver, not just at each timestep.

Overall, this method enables efficient representation of peroxy radical chemistry without adding an excessive number of reactions or transported tracers. This framework can be built on further, for example to parameterise the formation of RO_2 accretion products which are important for the formation of highly oxidised organic material (HOM) (Weber et al., 2020).

3.2 Merging with Stratospheric Chemistry

As both the MCM and CRI mechanisms are designed to simulate polluted boundary layer chemistry, they lack many reactions which are not relevant in the boundary layer but are important in the upper troposphere and stratosphere due to the differing photochemical conditions at different altitudes. The UKCA model is used as part of UKESM1 (Sellar et al., 2019) with a model top at 85 km in the standard configuration, therefore

it is essential that the chemical mechanism can adequately represent both tropospheric and stratospheric chemistry.

The CRIv2-R5 scheme was merged with the Stratospheric chemistry in UKCA, described by Morgenstern et al. (2009) and updated into the StratTrop mechanism by Archibald et al. (2020), to produce the new CRI-Strat mechanism (see Table 1). In total, 20 species and 121 reactions that are important for stratospheric chemistry were added. Some of the added reactions involve chemical species already present in the CRIv2-R5 mechanism. In all cases, imported reactions used the same rate coefficients or cross sections as the equivalent reactions in StratTrop. Full details of the CRI-Strat mechanism are given in Tables S2-S5 of the supplement.
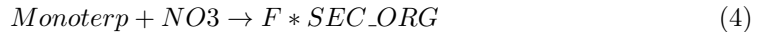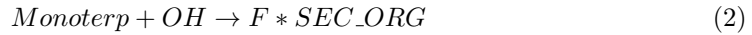
Photolysis reactions were added for methyl peroxy nitrate ($CH_3O_2NO_2$, MeO2NO2 in CRI-Strat) using the same cross sections as for HO_2NO_2 (Browne et al., 2011). The species $CH_3O_2NO_2$ is not part of the StratTrop mechanism but is an important reservoir for NO_x in cold temperatures and so photolysis of this species is needed to prevent accumulation in the upper troposphere and stratosphere. Reactions forming water vapour with a sizeable flux in the upper atmosphere were adjusted to ensure that H_2O was specified as a product; while chemical production of water vapour is typically neglected in the troposphere it forms an important part of the budget in the stratosphere.

3.3 Coupling with GLOMAP Aerosols

The UKCA model incorporates a modal representation of aerosol size distribution using the two-moment aerosol microphysics scheme from the Global Model of Aerosol Processes (GLOMAP-mode) (Mann et al., 2010) for all aerosol components (sulphate, sea-salt, black carbon and organic carbon, but not currently ammonium nitrate), with the exception of mineral dust which employs a bin scheme as described by Woodward (2001). GLOMAP-mode is fully coupled with the StratTrop mechanism in UKCA (Archibald et al., 2020) as described by (Mulcahy et al., 2020).

To couple the CRI-Strat mechanism to GLOMAP-mode aerosol, the standard Strat-Trop couplings have been mimicked wherever possible, except for secondary organic aerosol (SOA) and dimethyl sulphide (DMS) chemistry as discussed below. Because the oxidant fields are different in CRI-Strat, the production of aerosols may differ greatly between CRI-Strat and StratTrop. The species and reactions in CRI-Strat needed for coupling with GLOMAP-mode are marked with an [A] in supplementary Tables S2-S6. As the main focus of this paper is to evaluate changes in the gas phase due to implementation of the CRI-Strat mechanism, here we only document how the aerosol is coupled. Evaluating the changes to the aerosol fields and their impacts on atmospheric composition and climate will be the subject of a follow up paper.

Formation of SOA is parameterised in GLOMAP-mode through formation of the SEC_ORG tracer, which represents the extremely low volatility products of biogenic volatile organic compound (BVOC) oxidation. SEC_ORG does not undergo any further chemistry, and is either permanently condensed to the aerosol phase as organic aerosol or is lost via deposition processes. When the StratTrop mechanism is coupled with GLOMAP-mode aerosol, SEC_ORG is formed via the reactions:

$$Monoterp + OH \rightarrow F * SEC\_ORG \tag{2}$$

$$Monoterp + O3 \rightarrow F * SEC\_ORG \tag{3}$$

$$Monoterp + NO3 \rightarrow F * SEC\_ORG \tag{4}$$

with rate coefficients equal to the equivalent oxidation reactions of α-pinene with OH, O_3 and NO_3 respectively. The factor F represents the yield of SEC_ORG from Monoterp and is set at runtime to be equal to 26% for all of the above reactions, based on a 13% yield from α-pinene (Tunved et al., 2004; Spracklen et al., 2006) and doubled to account

for a lack of SOA production from isoprene and anthropogenic species (Mulcahy et al., 2020).

To simulate formation of SEC_ORG in the CRI-Strat mechanism, all of the AP-INENE and BPINENE initial oxidation reactions produce SEC_ORG at the same yield as the StratTrop reactions with Monoterp, in addition to all of the gas-phase products which are important for ozone chemistry (see supplementary Table S5). This method is not ideal as it does not conserve carbon. However, it is designed to produce a similar amount of SEC_ORG as the StratTrop mechanism in order to enable fair comparison of the gas-phase chemistry between the mechanisms and it serves as a placeholder until a more complete coupling between gas-phase chemistry and aerosol can be developed. Working on more explicit couplings between the organic gas-phase chemistry and aerosol routines is ongoing and will build on CRI version 2.2 (M. E. Jenkin, Khan, et al., 2019) and CRIv2.2 with Highly Oxygenated Organic Material (CRI_HOM)(Weber et al., 2020) versions of the mechanism. In the long term, this potential for more realistic chemical coupling between gas-phase organic chemistry and SOA formation is one of the key advantages of using a semi-explicit mechanism such as CRI-Strat over a simpler mechanism such as StratTrop.

Dimethyl sulphide (DMS) is a sulphur containing compound emitted in large quantities by natural sources and is a critically important source of SO_2, particularly in the preindustrial atmosphere, which can be oxidised to form sulphate aerosols (Andreae, 1990). The DMS chemistry used here is the same as in the CRIv2-R5 implementation in the WRF-Chem model (Archer-Nicholls et al., 2014) and uses the von Glasow and Crutzen (2004) DMS chemistry scheme. This description of multi-generational DMS oxidation is more comprehensive than that used in StratTrop (Archibald et al., 2020) and fits better with the complexity of the rest of the CRI-Strat mechanism. Evaluating and updating the DMS chemistry in both the CRI-Strat and StratTrop mechanisms is part of ongoing work.

3.4 Coupling with FastJ-X photolysis

The Fast-JX photolysis scheme implemented in UKCA calculates photolysis rates ("j" rates) for each reaction based on experimentally determined cross sections and quantum yields at a range of wavelength bins (Telford et al., 2013). The CRI-Strat mechanism includes many more photolysis reactions than StratTrop (128 compared to 60). However, most of the added species do not have experimentally determined photolysis cross sections and quantum yields. In the original CRI scheme, used in a box model, the photolysis rates for these species were calculated using a two stream isotropic photolysis scheme described by Hayman (1997). When the mechanism was ported to WRF-Chem (Archer-Nicholls et al., 2014), photolysis cross section and quantum yield data were adopted from those of species that were already available in WRF-Chem. However, for new species, a box model was used to generate photolysis rate profiles as a function of solar zenith angle. Profiles with similar shapes generated in WRF-Chem were then scaled to match the profiles from the box model. These scaling factors were then applied to the corresponding cross section and quantum yield data to calculate surrogate photolysis rates for the new species.

For this implementation, cross sections already available in UKCA are used for added photolysis reactions wherever possible, otherwise the surrogate cross sections and scaling factors used in the WRF-Chem implementation are applied. References for the photolysis cross-section data are given in Telford et al. (2013). Details of all photolysis reactions in the CRI-Strat mechanism are provided in supplementary Table S3.

3.5 Wet and dry deposition

There are many new species in the CRIv2-R5 mechanism which are efficiently wet and dry deposited but would otherwise have long chemical lifetimes in the atmosphere. The deposition of new species not included in the StratTrop mechanism is based on the functional group(s) of the species in question. The dry deposition rates and Henry's law coefficients used are described in more detail by O'Connor et al. (2014) and Archibald et al. (2020). Appropriate dry deposition velocities and Henry's Law coefficients were taken from those of existing species in the StratTrop mechanism with a similar functional group or structure; Table 2 shows which surrogate species are used for deposition rate coefficients for each additional species in CRI-Strat. In the case of a species fitting in more than one category, the class with the fastest deposition rates was used. This ensures that all species undergoing deposition are removed at an appropriate rate, but data for specific species can be updated in the future when experimental data becomes available.

4 Methods

4.1 Description of Model Setup

The experiments conducted in this study use the UM version 10.9. The model configuration is based on UKESM1, with 85 vertical levels using terrain-following hybrid height coordinates up to 85 km and a horizontal resolution of $1.25° \times 1.875°$ (N96) (Walters et al., 2019). All of the simulations are run using nudging of wind and temperature fields and prescribed sea surface temperatures (Telford et al., 2008) to the ERA-interim reanalysis product by ECMWF (Dee et al., 2011) to constrain all simulations to observed meteorological evolution so the evaluation can focus on how changes to the chemical mechanism affect atmospheric composition (Zhang et al., 2014). The model simulations run from 1 September 2008 to 1 January 2019, with the analysis period from 1 January 2010 to the end of the runs. Well mixed greenhouse gases are not emitted, rather carbon dioxide levels are set as a constant field while methane, nitrous oxide and CFCs are prescribed with constant lower boundary conditions, all at 2014 levels (Archibald et al., 2020).

4.2 Emissions

The emissions used in this study are those developed for the Coupled-Model Intercomparison Project 6 (CMIP6) (Collins et al., 2017). Anthropogenic and biomass burning emissions data for CMIP6 are from the Community Emissions Data System (CEDS), as described by Hoesly et al. (2018), and can be downloaded from `http://www.globalchange.umd.edu/ceds/ceds-cmip6-data/`. All of the experiments use repeated 2014 emissions as the closest to present day available in the inventories. Anthropogenic emissions are based on the Emission Database for Global Atmospheric Research (EDGARv4.3.1) (`http://edgar.jrc.ec.europa.eu/overview.php?v=431`) across the globe, incorporating more detailed regional datasets where available (Hoesly et al., 2018), while biomass burning emissions for the modern period are largely based on Global Fire Emissions Database version 4 with small fires (GFED4s) (Van Der Werf et al., 2017) and merged with other datasets as described by Van Marle et al. (2017). Combination of these datasets onto a unified grid is described by Feng et al. (2020). Offline biogenic emissions are derived from the Model of Emissions of Gases and Aerosols from Nature (MEGAN) version 2.1 (Guenther et al., 2012). Oceanic BVOC emissions are included from the POET inventory (Olivier et al., 2003).

Table 3 shows the mappings used to link the CEDS emissions to CRI-Strat. Lumping of raw NMVOC species to CRIv2-R5 speciation is based on methods described in (Watson et al., 2008). We also include equivalent mappings to the StratTrop scheme, as well as total global emissions for 2014 in TgC yr^{-1}.

Table 2. CRI-Strat species which undergo wet or dry deposition but do not exist in StratTrop do so using coefficients based on surrogate StratTrop species.

Compound class	Functional group(s) / molecule	Dry/wet/both	CRIv2-R5 species	StratTrop surrogate
Alcohols	-OH	Both	EtOH, i-PrOH, n-PrOH, AROH14, AROH17, ARNOH14, ARNOH17	MeOH
Aldehydes	-CHO	Dry	HOCH2CHO, CARB14, CARB17, CARB11A, UCARB10, UCARB12, NUCARB12, UDCARB8, UDCARB11, UDCARB14, TNCARB26, TNCARB10, TNCARB12,TNCARB11, CCARB12, TNCARB15, TXCARB24, ANHY, TXCARB22 UDCARB17	MeCHO
Carboxylic Acids	-CO$_2$H	Both	RCOOH25	MeCO2H
Glyoxals	2x -C(O)-	Both	CARB3, CARB6, CARB9, CARB12, CARB15	MGLY
Hydroxy-ketones	-OH and R(O)R'	Both	CARB7, CARB10, CARB13, CARB16	HACET
Hydroxy-nitrates	-OH and -ONO2	Dry	HOC2H4NO3, RN9NO3, RN12NO3, RN15NO3, RN18NO3, RU14NO3, RTN28NO3, RTX28NO3	ISON
Monoterpenes	C$_{10}$H$_{16}$	Dry	APINENE, BPINENE	Monoterp
Nitrate-carbonyls	-ONO$_2$ and -C(O)-	Both	NOA, NUCARB12, RTX24NO3, RTN25NO3, RTX22NO3, RTN23NO3	NALD
Peroxides	-OOH	Both	HOC2H4OOH, RN10OOH, RN13OOH, RN16OOH, RN19OOH, RN8OOH, RN11OOH, RN14OOH, RN17OOH, RU14OOH, RU12OOH, RU10OOH, NRU14OOH, NRU12OOH, RN9OOH, RN12OOH, RN15OOH, RN18OOH, NRN6OOH, NRN9OOH, NRN12OOH,RA13OOH, RA16OOH, RA19OOH, RTN28OOH, NRTN28OOH, RTN26OOH, RTN25OOH, RTN24OOH, RTN23OOH, RTN14OOH, RTN10OOH, RTX28OOH, RTX24OOH, RTX22OOH, NRTX28OOH	EtOOH
Peroxy Acids	-CO$_3$H	Both	EtCO3H, HOCH2CO3H	MeCO3H
Peroxyacyl Nitrates	-PAN	Dry	PHAN, RU12PAN, RTN26PAN	PAN

Table 3. Mapping of raw CMIP6 NMVOC emissions to CRI-Strat and StratTrop mechanisms, with total emitted carbon mass for 2014 from Anthropogenic, biomass burning and biogenic sources.

Raw emission classes	Anthropogenic TgC yr^{-1}	Biomass Burning TgC yr^{-1}	Biogenic TgC yr^{-1}	CRIv2-R5 Species	StratTrop Species
VOC1: Alcohols	0.4 \ 3.	3.5 \ 0.1	48.5 \ 9.5	MeOH \ EtOH	MeOH \ to MeOH
VOC2: Ethane	5.3	2.8	1.0	C2H6	C2H6
VOC7: Ethene	4.9	4.1	25.8	C2H4	to C2H6
VOC9: Ethyne	3.1	1.1	–	C2H2	to C2H6
VOC3: Propane	5.5	0.6	1.0	C3H8	C3H8
VOC8: Propene	3.0	3.5	14.	C3H6	to C3H8
VOC4-6: Butanes and higher alkanes	4.8	0.4	0.1	C4H10	N/A
VOC10: Isoprene	–	0.6	588	C5H8	C5H8
VOC11: Monoterpenes	–	1.2	94.7	67% to APINENE* \ 33% to BPINENE*	Monoterp†
VOC12: Other Alkenes and Alkenes	6.5	0.8	2.6	TBUT2ENE	N/A
VOC13: Benzene	6.1	2.0	–	BENZENE	N/A
VOC14: Toluene	7.0	3.9	86.5	TOLUENE	N/A
VOC15-17: Xylenes and higher aromatics	3.1	1.1	–	oXYLENE	N/A
VOC21: Formaldehyde	1.0	2.1	1.8	HCHO	HCHO
VOC22: Other Aldehydes	0.5	3.4	10.0	MeCHO	MeCHO
	0.6	0.8	2.0	EtCHO	to MeCHO
VOC23: Ketones	1.5	1.1	22.9	Me2CO	Me2CO
	1.0	0.9	0.5	MEK	to Me2CO
VOC24: Acids	–	0.5	1.4	HCOOH	N/A‡
	4.4	7.1	1.9	MeCO2H	
Total CRI:	70.5	40.6	900.6		
Total StratTrop:	27.9	23.9	710.6		

* Two to one split between APINENE and BPINENE emissions according to Guenther et al. (2012) and Sindelarova et al. (2014).
† In the StratTrop mechanism Monoterp only forms Sec_Org and does not contribute to ozone formation. Therefore, emissions mapped to Monoterp are not included in the total NMVOC emissions for the StratTrop mechanism.
‡ Acids have historically not been mapped to StratTrop mechanism in UKESM1 (Archibald et al., 2020), even though HCOOH and MeCO2H are existing species.

The CRI-Strat mechanism utilises a wider breadth of input NMVOC emissions, using almost all of the available data from the CEDS emission database, therefore has a greater amount of total carbon mass emitted compared to an equivalent StratTrop run. For anthropogenic emissions, the most significant changes are due to the addition of aromatic species and C_4 alkane/alkene emissions. For biogenic emissions, the largest change is that monoterpenes are mapped to the chemically reactive APINENE and BPINENE tracers in CRI-Strat, which undergo oxidation and contribute to ozone formation, whereas in StratTrop they are mapped to the MONOTERP tracer which is only considered as a precursor of SOA and does not contribute to ozone production). The total NMVOC emissions for the year 2014 using the CEDS emissions inventory are given in Table 3.

4.3 Model Simulations

Two base simulations are conducted, labelled StratTrop and CRI-Strat (Table 4). These use the emissions associated with their respective mechanism, as described in Table 3. The StratTrop simulation uses a slightly modified version of the mechanism, where the reactions of NO_3 + DMS and NO_3 + Monoterp were adjusted so that they conserved nitrogen, when previously they did not. These changes were made to enable a fair comparison between the mechanisms for Section 5.6. These changes have a minimal impact on the overall chemical composition in StratTrop and are explained in detail in Section S3 of the Supplement.

The treatment of emissions can be seen as an intrinsic part of a chemical mechanism. However, the emissions of additional NMVOC species in the CRI-Strat simulation which are not represented in StratTrop pose a dilemma when comparing the two mechanisms: are the differences between the simulations due to the different approaches in representing chemistry, there being more reactive carbon available in CRI-Strat, or a combination of these factors? Two additional simulations were therefore designed to better understand the effects of additional NMVOC emissions. A CRI-Strat run was conducted with identical emissions to the StratTrop base run (CRI_Emiss_ST) to isolate the changes just due to the chemical mechanism without any changes in emissions. The final CRI-Strat simulation only uses emissions from NMVOC emission classes that are also used by StratTrop, but these are mapped to the appropriate CRI-Strat species, hence it can be used to identify the effects of changing the speciation of NMVOC emissions without increasing the total carbon mass. The key difference is that C_2 and C_3 species are mapped into different species, hence this scenario is called speciated C2-C3 emissions (CRI_Emiss_C2C3). For example, emissions of ethane, ethene and ethyne are mapped to C2H6, C2H4 and C2H2 respectively in CRI_Emiss_C2C3, rather than being lumped to C2H6 as in the StratTrop and CRI_Emiss_ST scenarios. The MONOTERP tracer is unreactive in StratTrop (it can only be oxidised to form SEC_ORG and cannot contribute to ozone production), therefore all monoterpene emissions are mapped to MONOTERP in CRI_Emiss_ST and CRI_Emiss_C2C3, with the respective reactions copied over from StratTrop. The simulations are summarised in Table 4.

5 Results

In this paper, we focus on understanding how changes in chemistry affect gas-phase species which are important for describing the global tropospheric composition as drivers to climate: ozone, carbon monoxide, hydroxy radicals, methane lifetime and nitrogen oxides. We present a short evaluation against surface and remote sensing products, but the main focus is on comparing the performance of the CRI-Strat with the StratTrop mechanism, which is already well evaluated (Archibald et al., 2020), and on understanding how these changes are sensitive to the treatment of NMVOC emissions. While the changes in chemistry and oxidant fields are also expected to affect formation of aerosols, these influences will be explored in more detail in follow up studies.

Table 4. Summary of simulations.

Scenario Name	Chemical Mechanism	Emissions	Purpose
CRI-Strat	CRI-Strat	Standard CRI	Base CRI scenario
StratTrop	StratTrop	Standard ST	Base StratTrop scenario
CRI_Emiss_ST	CRI-Strat	Standard ST	Isolating effect of chemical representation without changes to emissions
CRI_Emiss_C2C3	CRI-Strat	Speciated C2-C3 emissions	Isolating effect of NMVOC speciation without changing total emitted mass

5.1 Model evaluation

5.1.1 Surface ozone

Lowest model level ozone concentrations from the base CRI-Strat and StratTrop model simulations are evaluated against the global dataset of rural surface ozone sensors compiled for the Tropospheric Ozone Assessment report (TOAR) (Schultz et al., 2017). The TOAR dataset compiles ozone measurements from surface station-based observations around the globe including data from regional and national air quality networks, as well as larger global collaborations.

The data used in this work are the gridded surface ozone datasets, which include mean surface ozone concentrations on a $2° \times 2°$ global grid. Schultz et al. (2017) also provide gridded station means separated by urban or rural classification, based on the population density, nightlight intensity, and OMI satellite NO_2 column. The model lowest level ozone concentration was evaluated against the rural mean surface ozone gridded dataset, because the relatively large grid size in the UKCA model ($1.25° \times 1.875°$, approximately 135 km horizontal grid spacing at the equator) means that urban-scale chemistry is not well resolved. In all comparisons with TOAR gridded data, the model output was regridded to the same $2° \times 2°$ grid as the TOAR data before analysis.

Figure 1 shows comparison of CRI-Strat and StratTrop model simulations with TOAR observations across the globe, grouped by region. Further plots comparing model output with TOAR data are included in the supplement Figures S6-S9. The CRI-Strat simulation has consistently higher surface ozone values across almost the entire world, with this increase most pronounced in populated regions such as Europe and East Asia. In more remote regions, the difference between the CRI-Strat and StratTrop simulations is much smaller. The CRI-Strat and StratTrop simulations follow similar seasonal trends, showing this variation is driven more by the parent model and shared traits, such as seasonal variation in emissions. In many regions, both simulations are low compared to observations in winter months and high in summer months. Due to CRI-Strat having higher ozone in general, the global summer high bias is greater in CRI-Strat (+12.6 ppbv) compared to StratTrop (+7.4 ppbv), but has a smaller negative bias in winter (-4.3 ppbv compared to -9.2ppbv). These results indicate that the CRI-Strat mechanism has a higher ozone production efficiency than StratTrop.

The high bias in surface summer ozone and low bias in winter are likely due to structural issues in using a coarse, global model as has been documented elsewhere (Young et al., 2013, 2018; Archibald et al., 2020). For example, the coarse horizontal resolution results in the emissions being smoothed and less heterogeneous, particularly around urban areas and large point sources, leading to greater mixing of NO_x and NMVOCs and ozone production, particularly in summer (Wild & Prather, 2006; Stock et al., 2014; Fenech et al., 2018). The low bias in winter, when local production is lower, may be due to in-
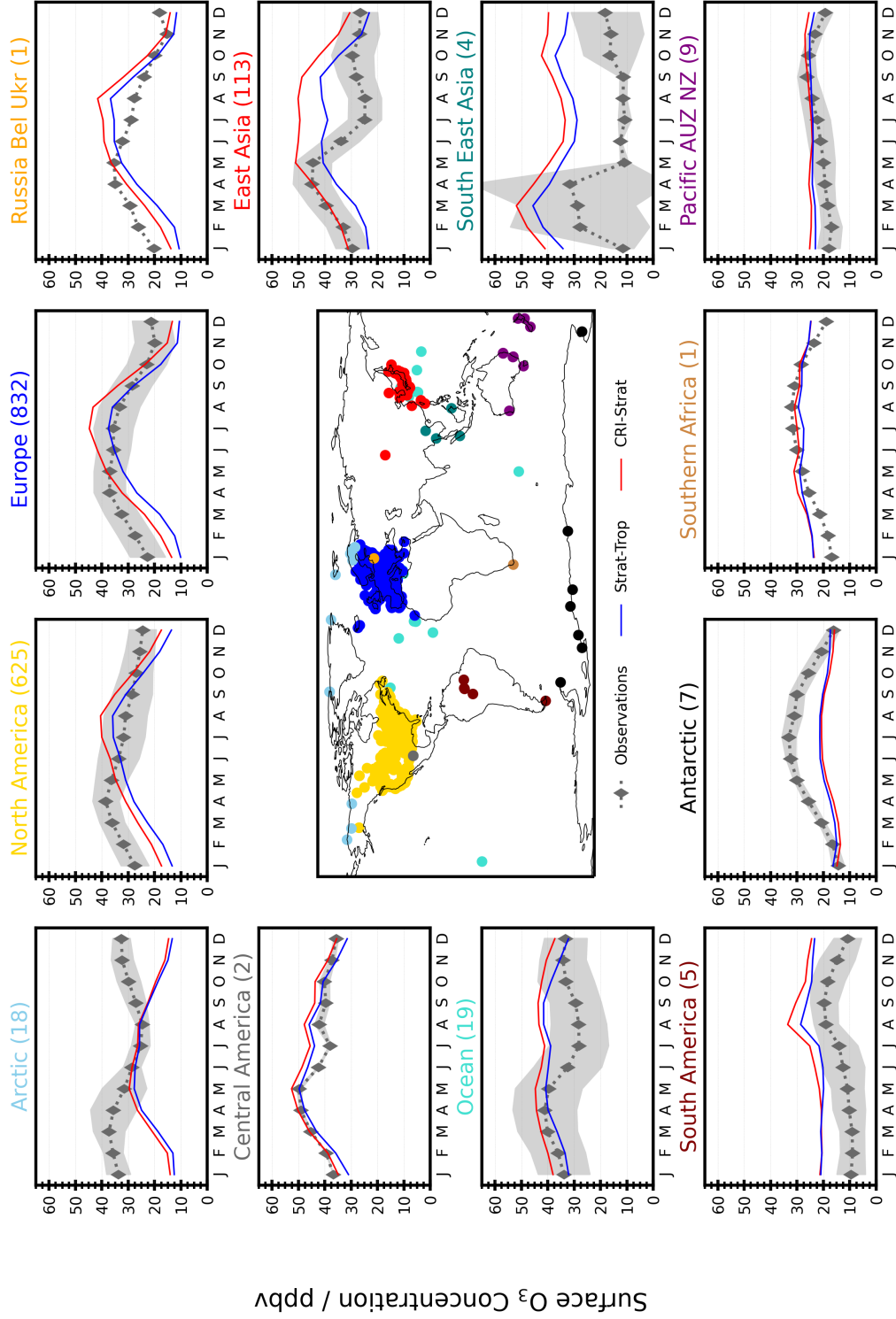
Figure 1. Monthly average surface ozone concentrations from low elevation rural sites on the TOAR network using data from 2010 to 2018. Data is grouped by region, with number of stations in each region given in brackets, and compared with corresponding locations from StratTrop (blue) and CRI-Strat (red) model simulations.

sufficient long range transport of ozone or loss due to deposition being too great. In some
regions, such as East Asia, the seasonal cycle in the model simulations is out of phase,
with the model runs showing peak ozone in the summer when the observations are at
their lowest. This is likely indicative of missing model processes, such as heterogeneous
chemistry or poor representations of local weather processes, such as monsoon cycles.
Any biases caused by such structural weaknesses in the parent model are common to both
mechanisms, but may be accentuated in CRI-Strat due to greater ozone production when
photochemical conditions allow. Given these issues, the higher bias in CRI-Strat com-
pared to the TOAR surface ozone observations likely more clearly reveal other biases in
the model which compensate for errors associated with the less accurate description of
the underlying chemistry in StratTrop.

5.1.2 Surface carbon monoxide

Modeled carbon monoxide (CO) surface fields are evaluated against the National
Oceanic and Atmospheric Administration (NOAA) climate Monitoring and Diagnostics
Laboratory (CMDL) dataset (Pétron et al., 2002), as shown in Figure 2. The NOAA data
are derived from regular *in situ* flask samples and screened for local pollution events. The
observational data evaluated here are calculated as a monthly average climatology de-
rived from observations made between 2010-15. The StratTrop simulation shows a low
bias at most sites in the Northern hemisphere, which are more influenced by anthropogenic
pollution, but is close to observed values in the tropics and over the southern hemisphere
which are more remote and dominated by biogenic and biomass burning emissions. These
effects have been documented elsewhere (Archibald et al., 2020). The CRI-Strat simu-
lation has greater CO at all sites and over all seasons compared to StratTrop. This re-
duces the size of the negative bias at northern hemisphere sites but creates a positive
bias over the remote southern hemisphere sites. The seasonal trends in both simulations
are similar, showing that these are more sensitive to model dynamics and seasonal vari-
ation in emissions than chemical mechanism. The higher CO in CRI-Strat is due to sec-
ondary production of CO from oxidation of the additional NMVOCs but this has mixed
effects on the comparison with observations, improving biases in the northern hemisphere
whilst making them worse in the southern hemisphere.

5.1.3 Tropospheric ozone column

Although surface ozone is a pressing concern for air quality, the influence of ozone
on climate is more dependent on ozone in the upper troposphere and the tropospheric
ozone burden (Bowman et al., 2013). We use two different monthly mean gridded satel-
lite data products to evaluate tropospheric column ozone (TCO) in the CRI-Strat and
StratTrop simulations. The OMI-MLS TCO monthly gridded data, determined by sub-
tracting the Microwave Limb Sounder (MLS) stratospheric column ozone (Waters et al.,
2006) from the Ozone Monitoring instrument (OMI) total column ozone (Dobber et al.,
2006), is available between 60°S-60°N with a horizontal resolution of 1°×1.25°, as de-
scribed by Ziemke et al. (2006, 2019). For comparison with OMI-MLS data (2010-2018),
the modelled TCO is calculated by vertically integrating the model ozone between the
surface and the tropopause (defined as 380K + 2 PV; Hoerling et al. (1993). The OMI
data (Boersma et al., 2007) were produced by the Remote-Sensing Group at Rutherford
Appleton Laboratory using a profile retrieval scheme developed first for GOME-2 (Miles
et al. 2015). Individual profiles were gridded on a monthly basis with a horizontal res-
olution of 1.5°×1.5° and a correction applied in each layer for bias with respect to ozoneson-
des which had been derived as a function of month of year and latitude (R. Siddans pri-
vate communication). For comparison with OMI data (2010-2017) in the surface-450 hPa
and 450-170 hPa layers, we use monthly, gridded averaging kernels and *a priori* infor-
mation to minimise vertical sampling differences between OMI and UKCA. Although
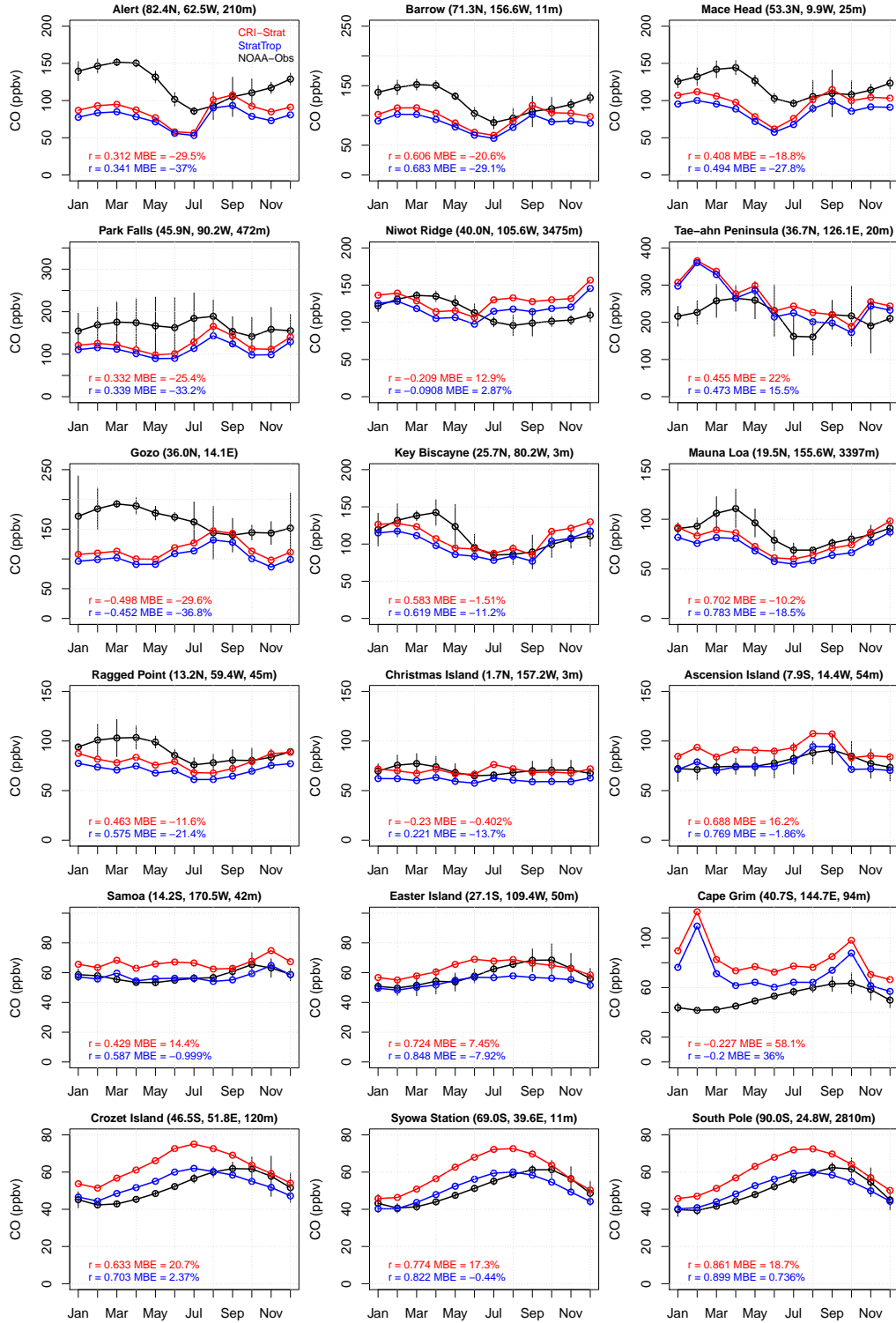potential issues with using monthly mean rather than individual averaging kernels can

Figure 2. Average surface CO concentrations from CMDL network (black) compared with CRI-Strat (red) and StratTrop (blue) model simulations, showing average seasonal variation, correlation coefficient and mean bias error over 2010-2018 evaluation period.

arise for certain species and instruments (von Clarmann & Glatthor, 2019), agreement between model and observation are found to be improved substantially through application of monthly mean averaging kernels in this analysis.

In Figure 3, average tropospheric ozone column is compared between the OMI-MLS satellite product and the CRI-Strat and StratTrop simulations. Differences in tropospheric ozone column between each of the model simulations are presented in supplementary Figure S10. The tropospheric ozone column is remarkably similar in the CRI-Strat and StratTrop simulations, both showing a similar high bias over the tropics and a low bias at high latitudes (Figure 3 (c, e)). The CRI-Strat and StratTrop simulations also have similar tropospheric ozone burden between 60°S and 60°N (303 Tg and 308 Tg respectively, compared to 301 Tg from OMI-MLS).

The seasonal zonal mean ozone in Figure 3 (b, d, f) is also more similar in the two model simulations compared to OMI-MLS. Both mechanisms show a clear high bias over the tropics throughout the year, with a strong peak between 0 and 30°N between March and June. In contrast, the satellite product has higher ozone column values around 40°N in June-July, with a slightly smaller peak around 30°S in October-November, a pattern not represented in the model simulations. Considering the large differences in surface ozone between the two mechanisms (Figure 1) it is perhaps surprising how similar the total tropospheric ozone is between the two mechanisms, and this is probably a sign that common model deficiencies (such as errors in emissions or transport) cause similar biases in both simulations. However, these tropospheric column comparisons may hide significant differences in vertical distribution of ozone.

The high bias in tropospheric ozone column seen over equatorial regions in both model simulations (Fig. 3 c-f) is absent in the lower troposphere (Fig. 4 c, e), but appears in the upper troposphere (Fig. 4 d, f). As the mechanisms show a similar bias in this region of the atmosphere, similar structural weaknesses must be causing the bias in both simulations, likely contenders being errors in lightning NOx emissions (Banerjee et al., 2014) or convective transport (Hoyle et al., 2011). CRI-Strat has higher ozone columns than StratTrop above polluted regions such as India and downwind of Europe, mostly in the lower troposphere, but has reduced ozone compared to StratTrop in the less polluted southern hemisphere (4 g, h).

5.2 Comparison of the ozone budget and processes in CRI-Strat and StratTrop

In this section, we investigate why tropospheric chemical composition differs between the CRI-Strat and StratTrop mechanisms. This is assessed using the base CRI-Strat and StratTrop simulations, and the two CRI-Strat simulations with modified NMVOC emissions (CRI_Emiss_ST and CRI_Emiss_C2C3). Collectively, these simulations allow us to explore the impact of changing chemistry without changing emissions, the difference attributable to explicit speciation of emissions, and the impact of the additional chemistry of C4 alkanes and alkenes, aromatics and monoterpene. Given that the StratTrop mechanism does not use a large fraction of the reactive carbon mass included in the input inventory, this analysis may also illustrate the causes of certain biases in the StratTrop mechanism and how these might be improved if it were to be modified to use a wider selection of NMVOC species, informing future development of this mechanism.

5.2.1 Ozone comparison

Boundary layer ozone is much higher over land in CRI-Strat compared to StratTrop, but is lower over remote oceans (Figure 5). Ozone levels are mostly lower in CRI_Emiss_ST and CRI_Emiss_C2C3 than StratTrop, but are higher over polluted regions. The variability in ozone is greater in CRI_Emiss_C2C3 than in CRI_Emiss_ST, and there are higher
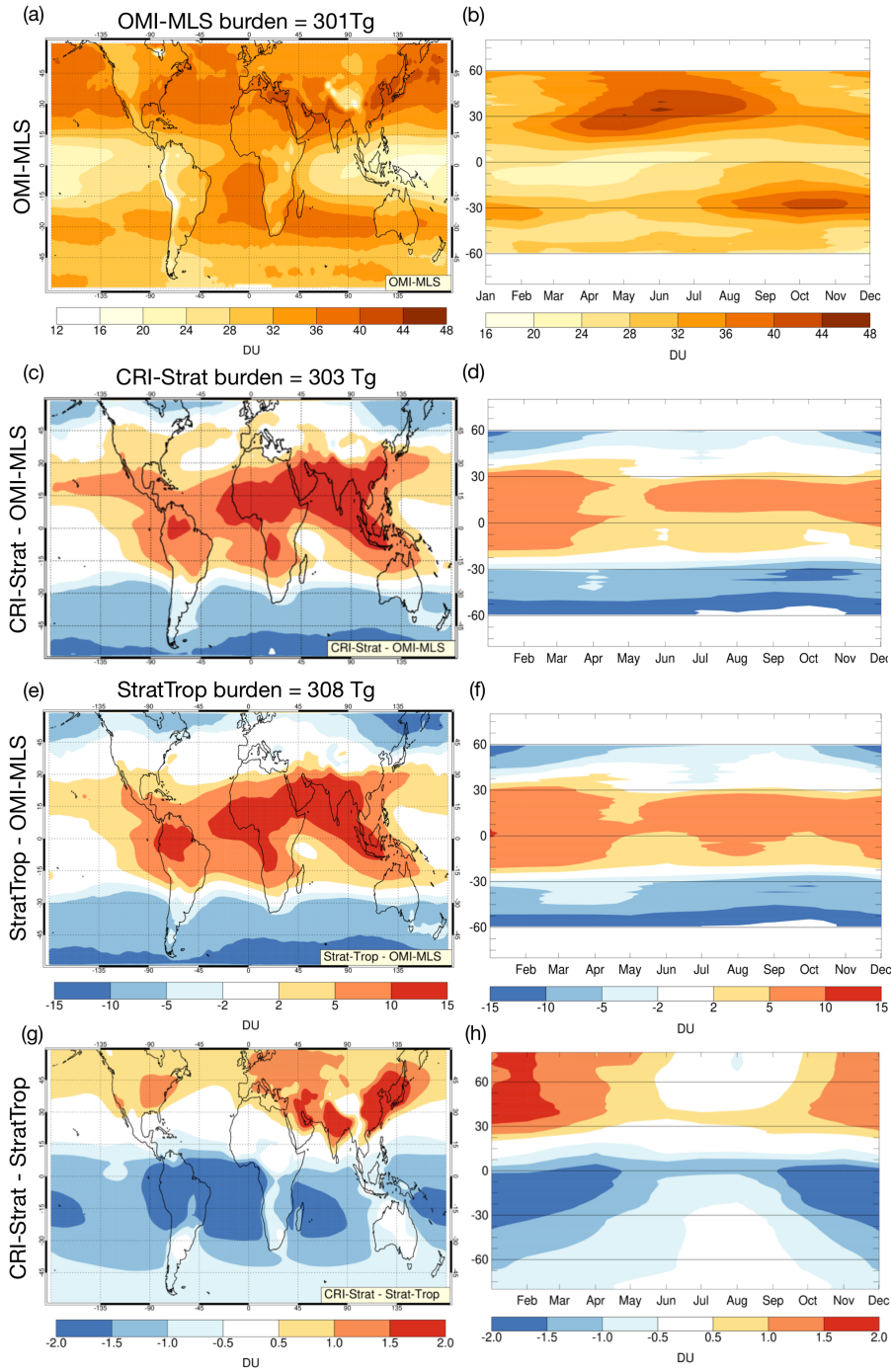
Figure 3. Map of tropospheric ozone column (DU) from OMI-MLS (a) and annual variation in zonal means (b), averaged between 2010-2018. Difference in tropospheric ozone column between CRI-Strat and OMI-MLS (c, d), between StratTrop and OMI-MLS (e, f), and between CRI-Strat and StratTrop noting different colour scale (g, h). Burdens given above panels a, c and e are calculated by summing ozone over the troposphere between 60°S to 60°N as this is the range covered by the OMI-MLS product.
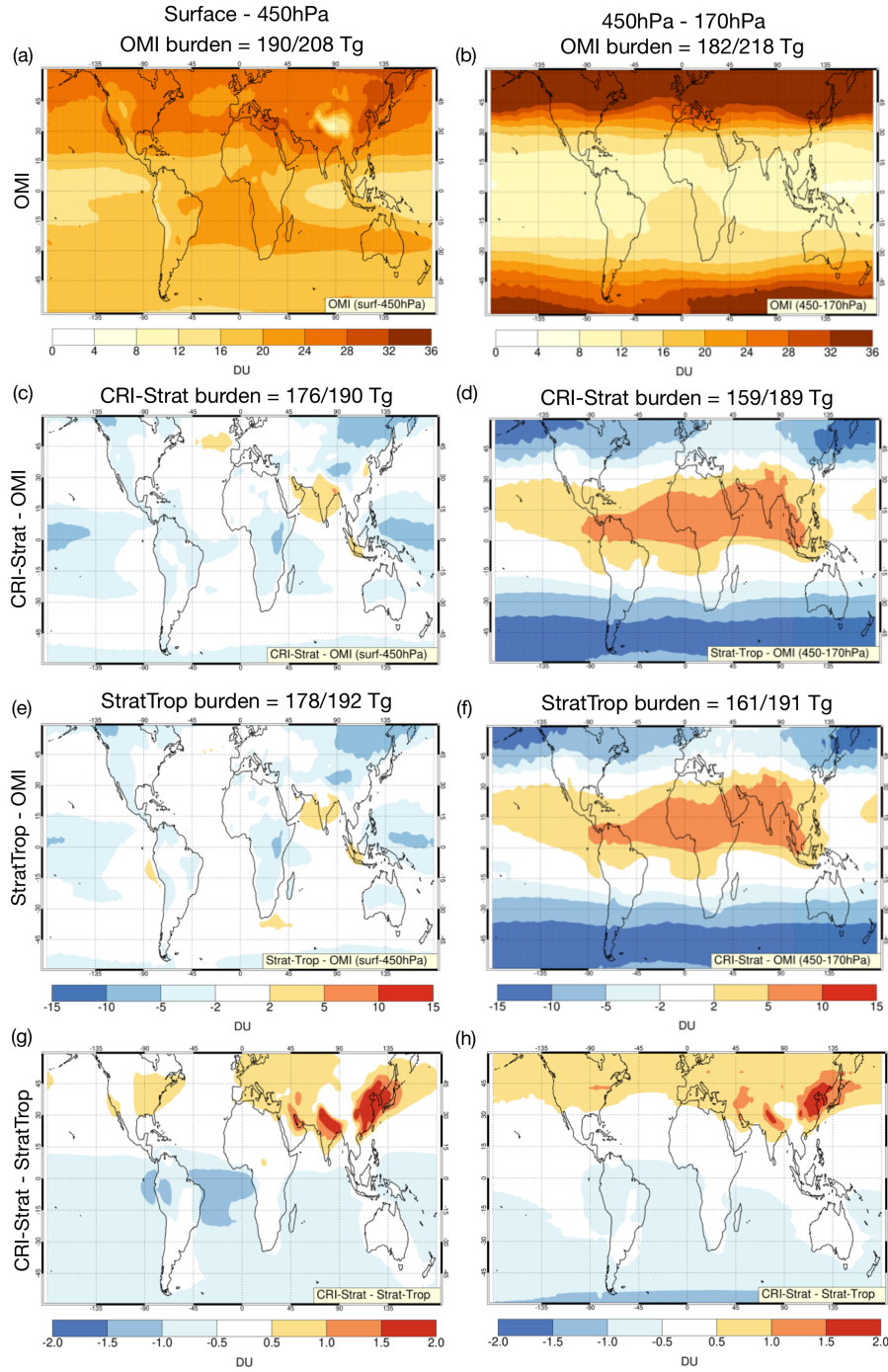
Figure 4. Ozone column between surface and 450 hPa from OMI satelite product as map (a) and from 450 to 170 hPa (b), averaged between 2010-2017. Difference in ozone column between CRI-Strat and OMI over respective pressure ranges (c, d), between StratTrop and OMI (e, f), and between CRI-Strat and StratTrop, noting different colour scale (g, h). Burdens are given over the respective pressure ranges for between 60°S to 60°N then over 90°S to 90°N.
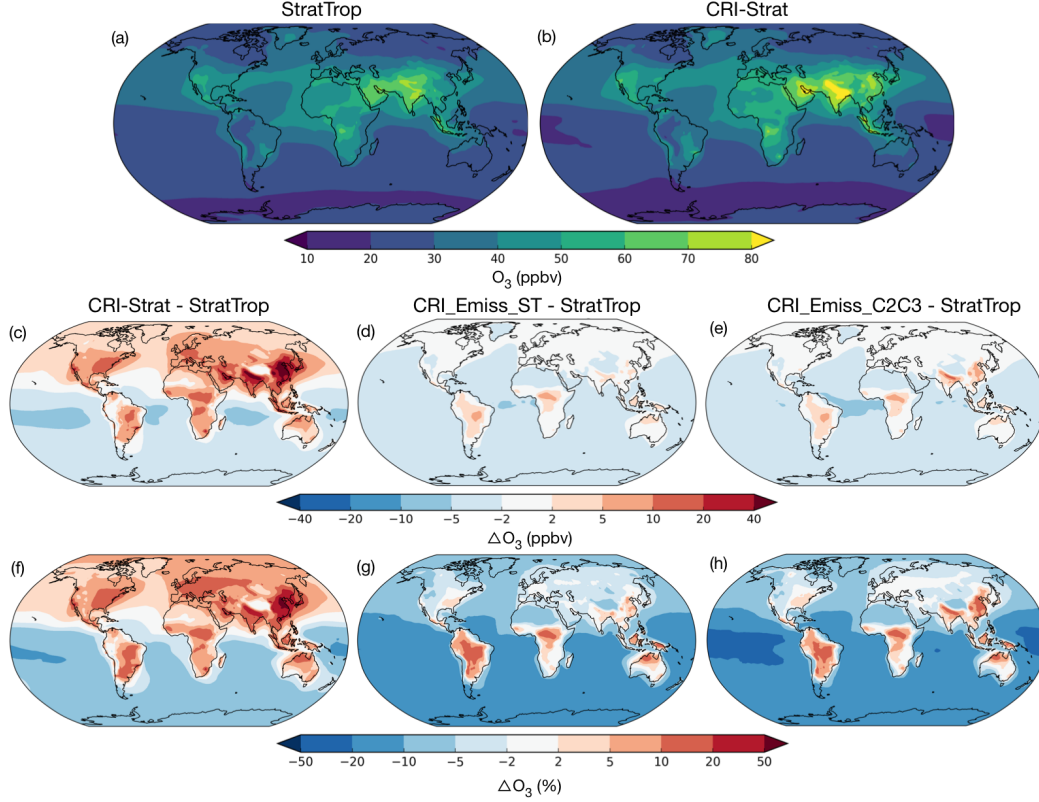
Figure 5. Mean ozone averaged over lower 1 km of the atmosphere in StratTrop (a) and CRI-Strat (b). Absolute difference (c-e) and relative difference (f-h) in ozone over lower 1 km of atmosphere between CRI-Strat and StratTrop (c, f), CRI_Emiss_ST - StratTrop (d, g), and CRI_Emiss_C2C3 - StratTrop (e, h).

ozone levels over highly populated regions such as the Indo-Gangetic plain but lower levels in remote regions. This is due to CRI_Emiss_C2C3 having emissions of alkenes such as C_3H_6 which are more reactive and have a higher ozone production efficiency than equivalent alkanes such as C_3H_8, but have shorter lifetimes and contribute less to ozone production downwind of sources (M. E. Jenkin et al., 2002).

Looking at the vertical distribution of ozone, high ozone levels in CRI-Strat are localised to the lower atmosphere in the northern hemisphere (Figure 6 (a, d)). Ozone concentrations are lower in the upper tropical troposphere and across the southern hemisphere. CRI-Strat has higher ozone in the lower stratosphere, but these differences are relatively small ($< 2\%$) and the largest fractional differences are in the lower atmosphere. In the CRI_Emiss_ST and CRI_Emiss_C2C3 scenarios, ozone levels are lower throughout most of the atmosphere, and the only region that shows similar zonal average ozone is the boundary layer between 30N and 60N (Figure 6 (b,c, e, f)). This demonstrates that the CRI-Strat mechanism is more efficient at producing ozone near emission sources, but that losses are greater in remote regions of the atmosphere.

The relationship between surface ozone and emissions is shown in the ozone isopleths in Figure 7. Ozone concentrations in all of the simulations are lower in NO_x-limited and VOC-limited regimes (in the bottom-right and top-left of each panel respectively), and drop slightly faster in CRI-Strat than StratTrop as NO_x emissions increase. Peak ozone concentrations in StratTrop occur in regions with lower VOC and NO_x emissions,
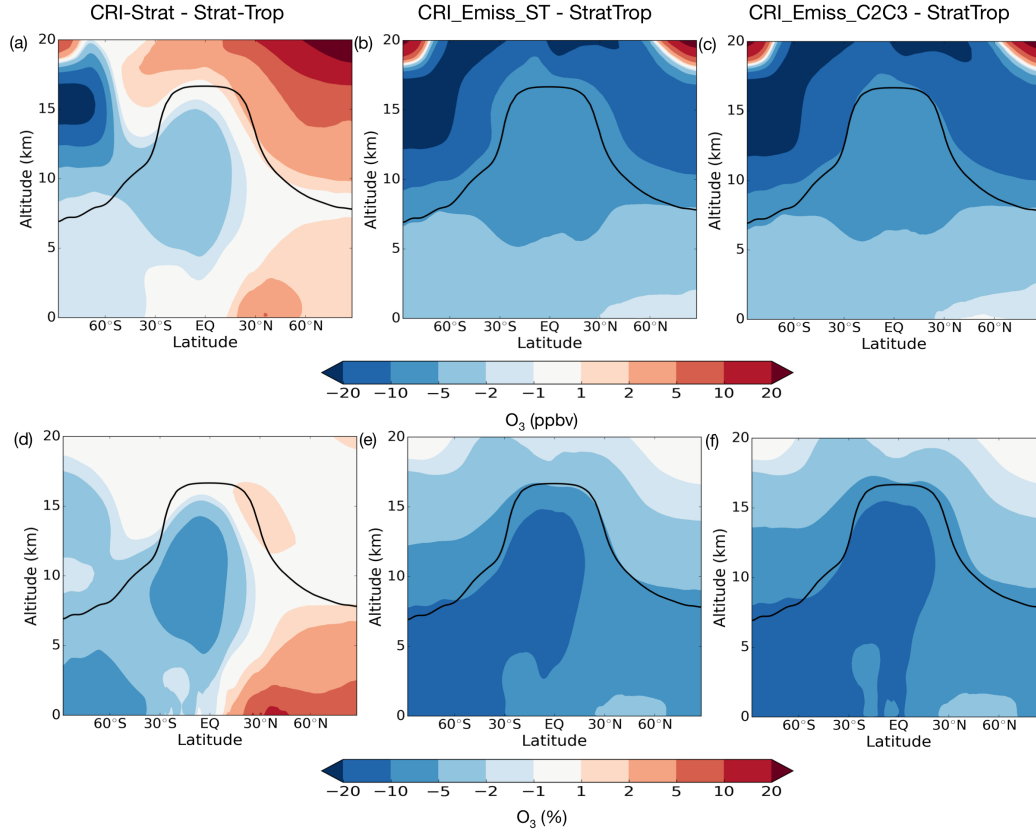
Figure 6. Zonal mean absolute difference (a-c) and percentage difference (d-f) in ozone between CRI-Strat and StratTrop (c, f), CRI_Emiss_ST - StratTrop (d, g), and CRI_Emiss_C2C3 - StratTrop (e, h). Black lines show average tropopause height over simulation period.
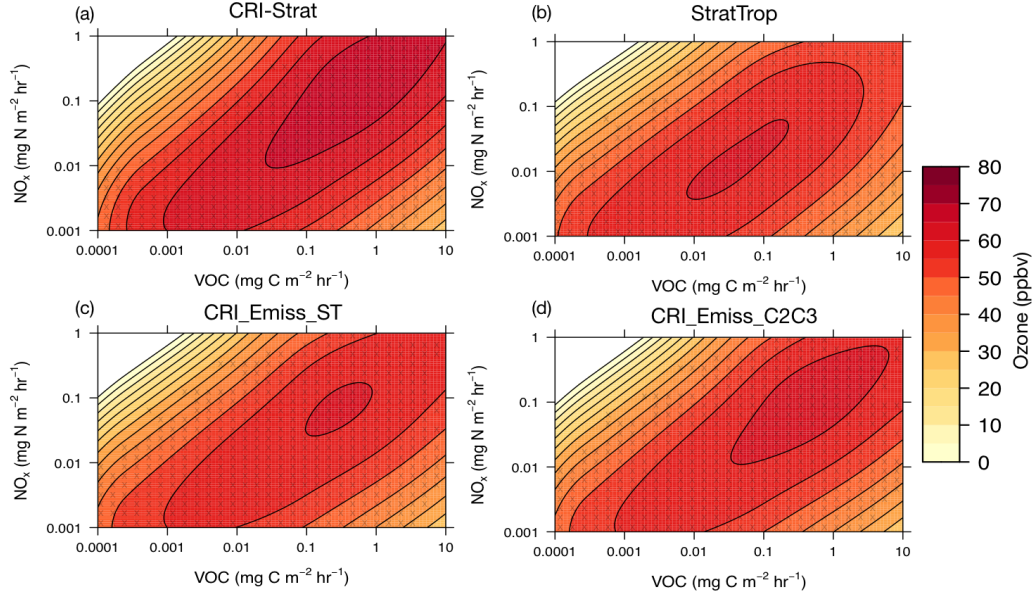
Figure 7. Ozone isopleths showing average surface ozone levels with respect to surface emissions of VOCs and NOx in StratTrop (a), CRI-Strat (b), CRI_Emiss_ST (c) and CRI_Emiss_C2C3 (d) model simulations. Isopleths have been drawn by mapping average surface ozone concentrations from each gridcell of each of the model simulations with NO and NMVOC emissions at each gridcell, then interpolating results to give a smooth field. Stippling shows regions of the phase space which have sufficient data from the model output.

between 0.01-0.1 mg C m^{-2}hr^{-1} and 0.01-0.1 mg N m^{-2}hr^{-1} respectively), and then drop off at high emission regions (Fig. 7 (a)). The CRI-Strat simulation has the highest ozone levels, with the increased NMVOC emissions spurring ozone production in more regions with high NO$_x$ emissions (Fig. 7 (b)). The CRI_Emiss_ST scenario shows a similar distribution to StratTrop but peak ozone levels occur in regions with higher emissions (Fig. 7 (c)). CRI_Emiss_C2C3 has peak ozone at even higher emission levels and the peak in ozone covers a broader region of the phase space, demonstrating that increased speciation of NMVOC emissions allows for greater ozone production in polluted regions as more is emitted as short lived, reactive compounds (Fig. 7 (d)).

5.2.2 Production and loss of ozone

To investigate these differences in ozone between the simulations, we present a full budget analysis of tropospheric ozone. Tropospheric production and loss of ozone is calculated using diagnostics which track the odd oxygen family, including NO$_2$ and its reservoir species, collectively known as O$_x$ (Wang et al., 1998):

$$O_x = O_3 + O + O(^1D) + NO_2 + 2NO_3 + 3N_2O5 + HONO_2 + HO_2NO_2 + PANs. \quad (5)$$

This definition of O$_x$ is based on the principle that the rate limiting step for ozone production following NO$_2$ photolysis is the conversion from NO to NO$_2$. Hence production (P$_{Ox}$) is primarily via the pathways HO$_2$ + NO, CH$_3$O$_2$ + NO and R'O$_2$ + NO (where R'O$_2$ is the sum of all peroxy radicals apart from CH$_3$O$_2$). Chemical loss of ozone (L$_{Ox}$) is defined as the sum of all chemical pathways which result in net loss of ozone, primar-

728   ily via reaction of $O(^1D)$ with water vapour and catalytic loss of O_3 with HO_x but also
729   via minor reaction pathways involving NO_3. Net ozone production is therefore defined
730   as the difference between chemical production and loss:

$$Net_{Ox} = P_{Ox} - L_{Ox} \qquad (6)$$

732   O_x is also lost via deposition (D_{Ox}), both directly through dry deposition of O_3 and in-
733   directly via deposition of NO_2 and its reservoir species. The final part of the budget is
734   from transfer of ozone from the stratosphere to the troposphere (S_{Ox}), which can be in-
735   ferred from the excess loss of ozone assuming no long-term changes in tropospheric bur-
736   den.

$$S_{Ox} = L_{Ox} + D_{Ox} - P_{Ox} \qquad (7)$$

738   Finally, the lifetime of O_x in the troposphere is calculated by dividing the total tropo-
739   spheric burden by the total loss via chemical sinks and deposition (Young et al., 2018).

$$\tau_{Ox} = B_{Ox}/(L_{Ox} + D_{Ox}) \qquad (8)$$

741   In the CRI-Strat simulation, ozone production is much higher than StratTrop in
742   the lower atmosphere, but also in most of the troposphere between 60°S and 90°N (Fig.
743   8 (a) and supplementary Figure S11). The only region where StratTrop has faster pro-
744   duction is in the southern upper tropical troposphere. In CRI_Emiss_ST and CRI_Emiss_C2C3,
745   ozone production is even more concentrated in the boundary layer, with much less pro-
746   duction than StratTrop in the upper troposphere (Fig. 8 (b, c)). However, all simula-
747   tions using the CRI-Strat mechanism have greater ozone loss over most of the troposphere
748   (Fig. 8 (d-f)), so that the main region of greater net ozone production is in the bound-
749   ary layer and there is a layer of net loss immediately above (Fig. 8 (g-i)). As shown in
750   Supplementary Figure S12, the difference in distribution of L_{Ox} is almost identical to
751   the flux through the $O(^1D) + H_2O$ reaction, one of the reactions that has different re-
752   action rate coefficients between the mechanisms. This reaction drives a large component
753   of the ozone changes between the mechanisms.

754   Table 5 gives an overview of the tropospheric ozone budget, production and loss
755   terms. While CRI-Strat and StratTrop have similar total tropospheric ozone burdens
756   of 331.8 Tg and 336.8 Tg respectively, the burdens of CRI_Emiss_ST and CRI_Emiss_C2C3
757   are both around 30 Tg lower. Compared to the TOAR model intercomparison (Young
758   et al., 2018), the tropospheric ozone burdens in the StratTrop and CRI-Strat simulations
759   are within the model interquartile range (320-370 Tg), whereas CRI_Emiss_ST and CRI_Emiss_C2C3
760   are below that range. Gaudel et al. (2018) calculate total ozone burdens between 333
761   and 345 Tg for the 2010-2014 period from satellite products which can observe all lat-
762   itude bands, overlapping with StratTrop and slightly above CRI-Strat but much higher
763   than CRI_Emiss_ST and CRI_Emiss_C2C3. Ozone production efficiency (OPE, defined
764   as moles of O_x produced per mole of NO_x emitted) is also higher in CRI-Strat (31.4) than
765   StratTrop (27.2).

766   The lifetime of ozone in all of the simulations using CRI-Strat chemistry is much
767   shorter (17.3-17.5 days) than with StratTrop (19.8 days), hence the lower ozone in CRI_Emiss_ST
768   and CRI_Emiss_C2C3 likely reflects the shorter lifetime of O_x. However, the CRI-Strat
769   simulation has a similar ozone burden to StratTrop because increased production com-
770   pensates for the increased losses. In fact, the lifetime of ozone in all of these simulations
771   is short compared to previous analysis (e.g. 22.3 ± 2.0 days from Young et al. (2013),
772   although these were for the year 2000 rather than 2014). Note also that the lifetime cal-
773   culation is dependent on the definition of O_x, for example Bates and Jacob (2020) find
774   O_3 lifetimes of approximately 75 days as they do not consider the $O(^1D) + H_2O$ reac-
775   tion to cause net loss of O_x. The short lifetimes could partly explain why both CRI-Strat
776   and Strat-Trop have lower ozone column values at high latitude than OMI-MLS (Fig-
777   ure 3), as insufficient ozone is transported from the tropics, where production is high-
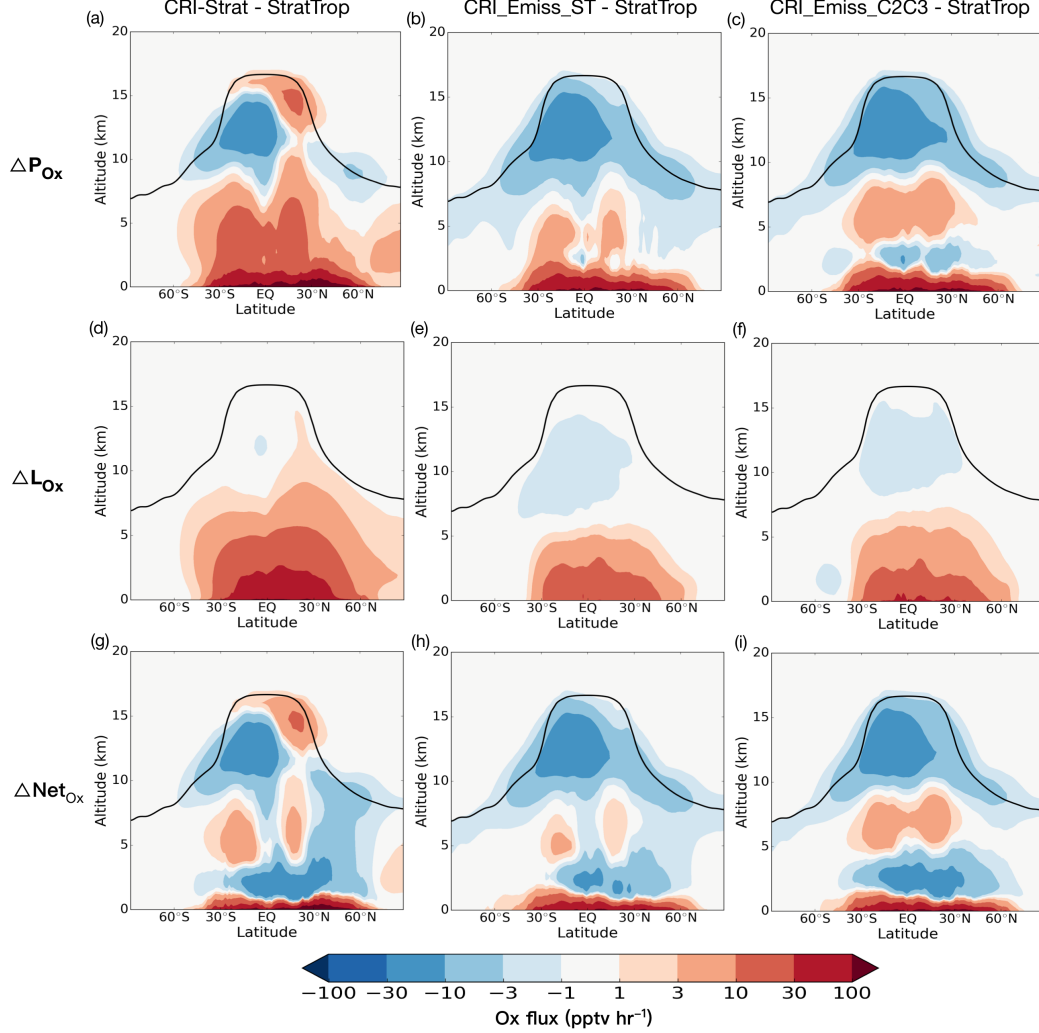778   est.

Figure 8. Zonal mean difference in chemical production of Ox between CRI-Strat and Strat-Trop (a), CRI_Emiss_ST and StratTrop (b), and CRI_Emiss_C2C3 and StratTrop (c) over 2010-2018 simulation period. Zonal mean difference in chemical loss of Ox between CRI-Strat and StratTrop (d), CRI_Emiss_ST and StratTrop (e), and CRI_Emiss_C2C3 and StratTrop (f). Zonal mean difference in net chemical production of Ox between CRI-Strat and StratTrop (g), CRI_Emiss_ST and StratTrop (h), and CRI_Emiss_C2C3 and StratTrop (i). Black lines show average tropopause height over simulation period.

Table 5. Overview of Ox burden, lifetime, ozone production efficiency (OPE), chemical production, chemical loss, deposition and inferred stratosphere to troposphere transfer. Values in brackets give fraction of total chemical production for the production terms and fraction of total losses ($L_{Ox} + D_{Ox}$) for the chemical loss and deposition terms.

		CRI-Strat	StratTrop	CRI_Emiss_ST	CRI_Emiss_C2C3
O_3 burden (Tg)		**331.9**	**336.8**	**308.0**	**306.8**
O_x lifetime (days)		17.3	19.8	17.5	17.4
NMVOC emissions (Tg C year^{-1})		1012	762	762	762†
OPE (mole$_{O_3}$ mole$_{NO_x}^{-1}$)		31.4	27.2	28.7	28.9
Chemical production (P_{Ox})	**Total**	**6624**	**5725**	**6057**	**6092**
(Tg O_3 year^{-1})	$HO_2 + NO$	4152 (62.7%)	3853 (67.3%)	3886 (64.2%)	4001 (65.7%)
	$CH_3O_2 + NO$	1540 (23.3%)	1285 (22.5%)	1452 (24.0%)	1419 (23.3%)
	$R'O_2 + NO$	882 (13.3%)	545 (9.5%)	676 (11.2%)	629 (10.3%)
	Other*	64.5 (0.7%)	41.3 (0.7%)	41.5 (0.7%)	43.2 (0.7%)
Chemical loss (L_{Ox})	**Total**	**5853**	**5128**	**5355**	**5380**
(Tg O_3 year^{-1})	$O(^1D) + H_2O$	3196 (45.5%)	2660 (42.9%)	3022 (47.1%)	3005 (46.6%)
	$HO_2 + O_3$	1713 (24.4%)	1596 (25.7%)	1498 (23.4%)	1513 (23.5%)
	$OH + O_3$	708 (10.1%)	714 (11.5%)	667 (10.4%)	680 (10.6%)
	O_3 + Alkene	160 (2.3%)	96.5 (1.6%)	115 (1.79%)	129 (2%)
	Other‡	76.3 (1.1%)	61.5 (1.0%)	53.1 (0.8%)	52.6 (0.8%)
Deposition (D_{Ox})	**Total**	**1164**	**1081**	**1061**	**1068**
	O_3 dry dep	974 (13.9%)	896 (14.4%)	872 (13.6%)	878 (13.6%)
	NO_y dep	190.3 (2.7%)	185 (3.0%)	189 (2.95%)	190 (2.94%)
Inferred STT (Tg O_3 year−1)		394	483	361	355

$\dagger$ Same carbon emission mass as StratTrop but different speciation.

* "Other" O_x production channels are the sum of inorganic acid oxidation, $RONO_2$ oxidation and $RONO_2$ photolysis.

$\ddagger$ "Other" O_x loss channels are the sum of $O(^3P) + O_3$, $O^3P + NO_2$, $N_2O_5 + H_2O$ and NO_3 chemical losses.

The ozone production and loss terms for CRI-Strat (6624 and 5853 Tg yr^{-1} respectively) are both much higher than for StratTrop (5725 and 5128 Tg yr^{-1}), and are higher than most models from the TOAR assessment (Young et al., 2018). It has been noted before that models with representation of higher aromatics and monoterpenes have high P_{Ox} and L_{Ox} terms (Porter et al., 2017), but the calculation of the net chemical tendency $(P_{Ox} - L_{Ox})$ shows that the CRI-Strat results in a greater overall propensity to form ozone in spite of the emissions of NMVOCs (c.f. StratTrop and CRI_Emiss_ST experiments Table 4). The P_{Ox} and L_{Ox} terms in CRI_Emiss_ST and CRI_Emiss_C2C3 are very similar to each other, in both cases higher than StratTrop and lower than the base CRI-Strat run. There is a general trend for "hotter" chemistry - more ozone is produced and lost - in all of the simulations using the CRI-Strat chemical mechanism. We can also say that the addition of higher NMVOC emissions has a larger impact on the ozone budget (CRI-Strat vs CRI_Emiss_ST and CRI_Emiss_C2C3) than the improved speciation of NMVOC emissions (CRI_Emiss_ST vs CRI_Emiss_C2C3).

The increase in ozone production in CRI-Strat occurs over all channels, but the largest relative increase is via $R'O_2 + NO$ (882 Tg yr^{-1}), which is over 50% larger in CRI-Strat than in StratTrop (545 Tg yr^{-1}), partly because there is more $R'O_2$ in CRI-Strat. The CRI_Emiss_ST simulation shows its largest increase in production compared to StratTrop via the $R'O_2 + NO$ channel, as well as the $CH_3O_2 + NO$ channel, whereas in CRI_Emiss_C2C3 it is via the $HO_2 + NO$ channel. Note though that the increased production via $HO_2 + NO$ and $CH_3O_2 + NO$ is also linked to oxidation of larger NMVOCs, as many reactions produce secondary HO_2 and CH_3O_2 as larger molecules are oxidised.

Chemical loss of O_x via the $O(^1D) + H_2O$ channel is greater in CRI-Strat (3196 Tg yr^{-1}) than in StratTrop (2660 Tg yr^{-1}). In addition, the CRI_Emiss_ST and CRI_Emiss_C2C3 scenarios have similar losses via this channel (3022 Tg yr^{-1} and 3005 Tg yr^{-1} respectively) to the base CRI-strat simulation, scaling linearly with ozone burden. The $O(^1D) + H_2O$ pathway is the primary driver behind why O_x lifetime is much shorter in the CRI-Strat chemical mechanism compared to StratTrop. This is down to both the reaction rate coefficients for the hydroxyl radical producing $O(^1D) + H_2O \rightarrow 2OH$ reaction being greater in CRI-Strat than in StratTrop, and the stabilising reaction $O(^1D) + M \rightarrow O(^3P) + M$ is smaller, which collectively result in excited $O(^1D)$ being about 25% more likely to react with H_2O than stabilise with M for a given concentration of water vapour (see Figure S2 and Section S4 in the supplement for details).

5.3 Hydroxyl and Hydroperoxyl Radicals

The hydroxyl radical (OH) is the major oxidant in the troposphere for almost all NMVOC species. Together with the hydroperoxyl radical (HO_2) it forms the HO_x family ($HO_x = OH + HO_2$). Zonal means of OH and HO_2 from the StratTrop simulation and differences to other simulations are shown in Figure 9. All of the simulations with CRI-Strat chemistry show a bimodal pattern in OH of high levels in the lower troposphere and low levels in the upper troposphere compared to StratTrop (Fig. 9 (c-e)), and a pattern of more HO_2 in both the lower and upper troposphere (Fig. 9 (f-h)). Total HO_x, which is roughly equal to HO_2, is much higher in all of the simulations using CRI-Strat chemistry than StratTrop (Fig. 9 (f-h)), which is unsurprising given the main source is the $O(^1D) + H_2O$ reaction which we already know has a much higher flux in CRI-Strat than StratTrop (Table 5).

In the lower atmosphere, which has higher O_3 in the CRI-Strat simulation and is abundant with water vapour, we have greater HO_x production and more OH and HO_2. There are also more $O_3 + Alkene$ reactions in CRI-Strat, which produce OH, and HO_2 is produced as a byproduct of many VOC oxidation and photolysis reactions. Together, these differences lead to the "hotter" chemistry in CRI-Strat.
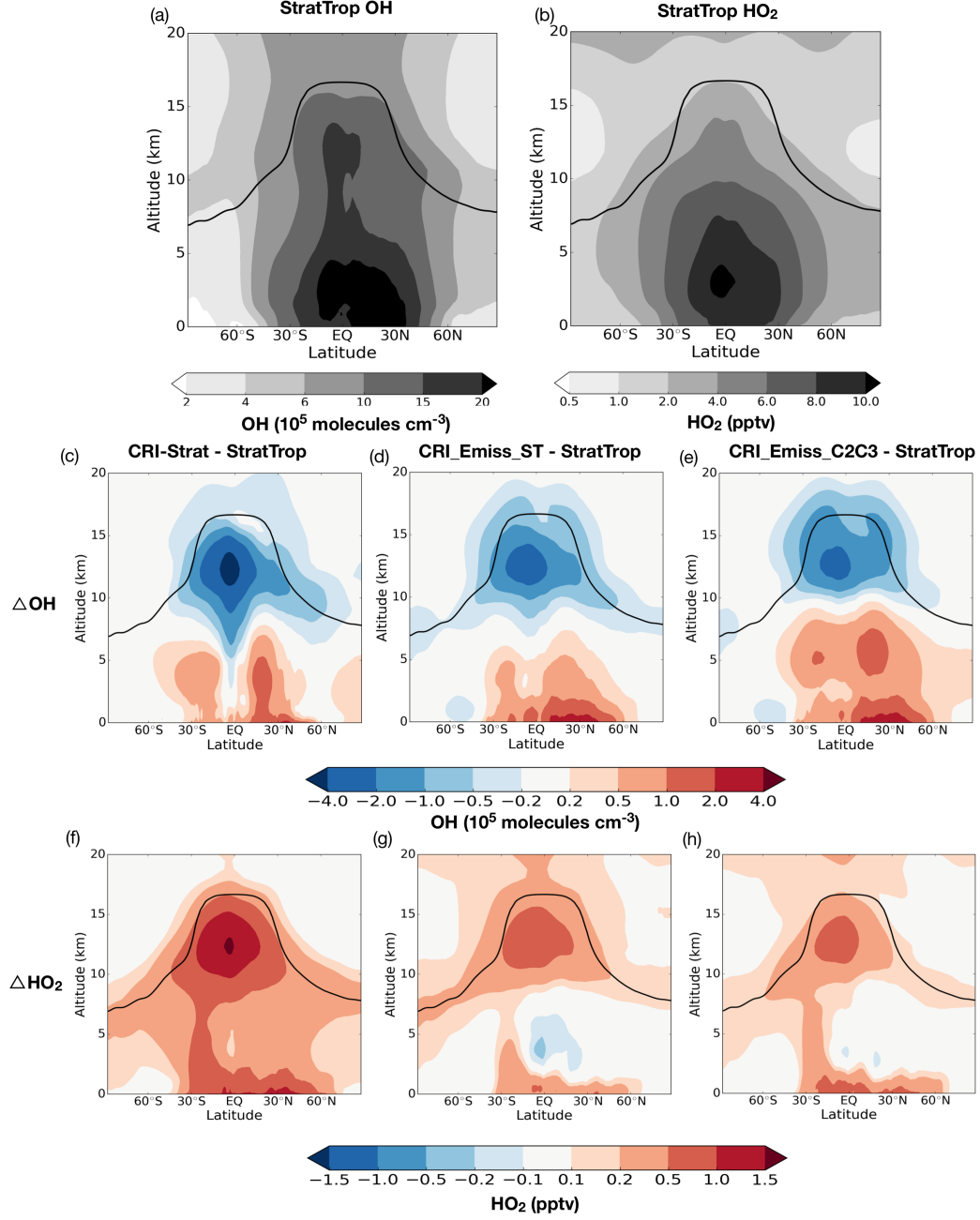
Figure 9. Zonal mean OH (a) and HO$_2$ (b) in StratTrop simulation. Differences in zonal mean OH and HO$_2$ between CRI-Strat and StratTrop (c, f), CRI_Emiss_ST and StratTrop (d, g), and CRI_Emiss_C2C3 and StratTrop (e, h). Black lines show average tropopause height over simulation period.

Table 6. Overview of mass weighted annual average tropospheric HOx concentrations, OH northern hemisphere to southern hemisphere ratio, OH : HO$_2$ ratio, methane lifetime with respect to OH and HO$_2$ + HO$_2$ flux.

	CRI-Strat	StratTrop	CRI_Emiss_ST	CRI_Emiss_C2C3
[OH] (10^6 molecules cm^{-3})	1.335	1.339	1.348	1.375
OH NH:SH ratio	1.38	1.35	1.4	1.4
[HO$_2$] (pptv)	6.27	5.90	6.02	6.06
OH : HO$_2$ ratio (%)	1.49	1.67	1.61	1.63
CH$_4$ lifetime W.R.T. OH (years)	7.77	8.13	7.71	7.60
HO$_2$ + HO$_2$ flux (P mole year^{-1})	60.5	32.2	38.8	39.9

In the upper troposphere, OH concentrations are much lower in CRI-Strat compared to StratTrop for a number of reasons. It is less moist than the lower atmosphere and away from emission sources of short-lived alkenes (which can make OH), hence primary OH production is lower. However, CRI-Strat has more formaldehyde than StratTrop and other carbonyls which can be photolysed in the upper troposphere to produce HO$_2$. CRI-Strat has more long-lived NMVOCs and CO in the upper troposphere which primarily react with OH converting it into HO2. Ozone levels in the upper troposphere are also lower in CRI-Strat. Hence CRI-Strat has more HO$_x$ in the upper troposphere, but a greater proportion is as HO$_2$ and there is less OH than in StratTrop.

Overall, CRI-Strat has slightly lower average OH concentration than StratTrop, whereas the CRI_Emiss_ST and CRI_Emiss_C2C3 simulations have more OH overall than the base CRI-Strat and StratTrop simulations (Table 6). Hence, given the same emissions the CRI-Strat mechanism produces more HO$_x$ than StratTrop, but this is countered by the additional NMVOCs in the full CRI-Strat mechanism which primarily react with OH, converting it into HO$_2$, leading to a lower OH : HO$_2$ ratio in CRI-Strat. The total HO$_2$ + HO$_2$ flux, a major sink of HO$_x$ in the atmosphere, is almost twice as high in CRI-Strat than in StratTrop due to both the increase in HO$_2$ and a faster reaction rate (see supplementary Figures S2 and S4).

The methane (CH$_4$) lifetime is slightly shorter in CRI-Strat than in StratTrop, even though OH is higher in StratTrop. The reason is because the OH + CH$_4$ reaction rate coefficient is slightly faster in CRI-Strat (see Figure S5 in the supplement). While this difference has little impact on the concentration of CH$_4$, because this is set by surface boundary conditions, it influences tropospheric chemistry because CH$_4$ is a major source of the methyl peroxy radical (CH$_3$O$_2$), the most abundant peroxy radical and an important component of the tropospheric ozone forming process (Table 5).

5.4 Carbon Monoxide

Carbon monoxide (CO) is important as the main chemical sink for OH, converting it into HO$_2$, and as a toxic air pollutant in its own right. It is produced from both primary emission sources, generally from incomplete combustion of biomass and fossil fuels, and secondary production from the oxidation of VOCs (Grant et al., 2010).

The total tropospheric burden of CO is over 50 Tg higher in CRI-Strat compared to StratTrop, and the CRI_Emiss_ST and CRI_Emiss_C2C3 simulations also have higher CO burdens (Table 7). The CO lifetime varies linearly with OH concentration between the simulations (Table 6), as the OH + CO reaction occurs at the same rate in both mechanisms, and so is slightly longer in CRI-Strat as it has slightly less OH overall compared
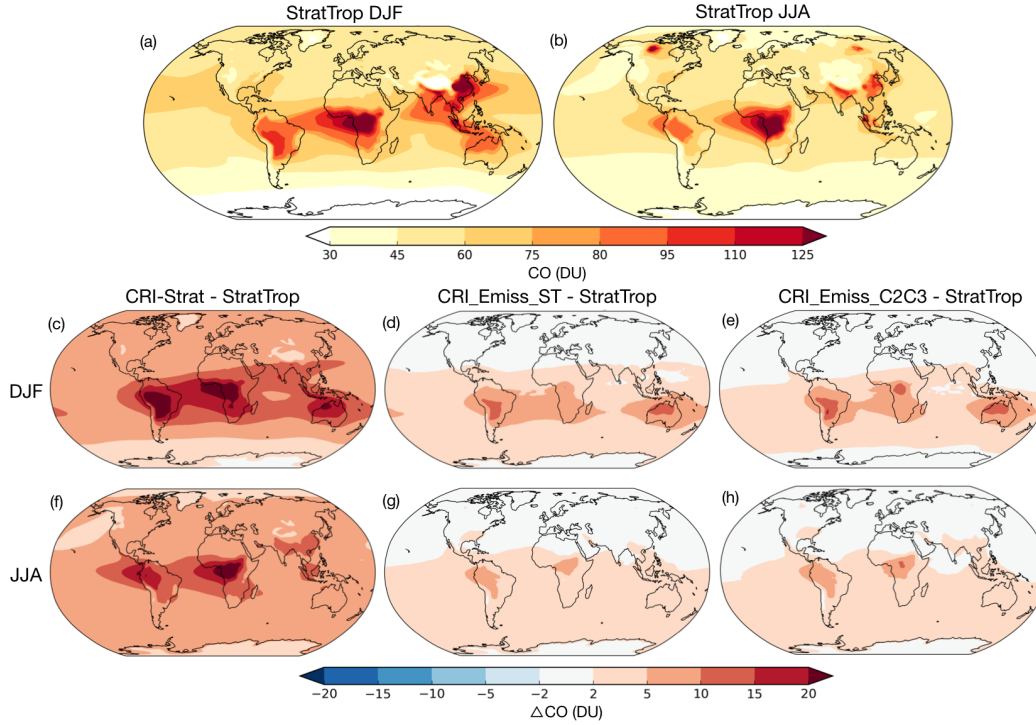
Figure 10. Average tropospheric column CO in StratTrop simulations for DJF (a) and JJA (b). Differences in tropospheric CO column in DJF and JJA between CRI-Strat and StratTrop (c, f), CRI_Emiss_ST and StratTrop (d, g), and CRI_Emiss_C2C3 and StratTrop (e, h).

to StratTrop. As all of the simulations use the same primary CO emissions, the differences in CO burden are due to secondary production and oxidant profiles. Although most of this secondary production occurs via formaldehyde (HCHO) oxidation and photolysis channels, there is a large increase in contribution from other channels in CRI-Strat compared to StratTrop (these being oxidation and photolysis of larger carbonyls, O_3+alkene reactions and PAN oxidation). The increase in CO production from HCHO and other channels is also apparent to a lesser extent in the CRI_Emiss_ST and CRI_Emiss_C2C3 scenarios. The more explicit NMVOC degradation chemistry in the CRI-Strat mechanism produces more HCHO and other oxidised NMVOCs, which go on to form CO as they are further oxidised and undergo photolysis.

The bulk of the additional CO burden is in the southern hemisphere downwind of regions with high BVOC emissions, such as the Amazon, Central Africa and Australia (Fig. 10). In CRI_Emiss_ST and CRI_Emiss_C2C3, increases in CO column are localised to these regions and downwind of them (Fig. 10 (d, e, g, h)), implying that the primary cause of increased CO is the more explicit, multigenerational representation of isoprene degradation in the CRI-Strat mechanism. The base CRI-Strat simulation has much more CO over these BVOC dominated regions and a background increase in column CO of around 5-10 DU across almost the entire world, including the northern hemisphere (Fig. 10 (c, f)). This is due to additional CO production from degradation of higher NMVOCs emitted by anthropogenic sources, as well as from the explicit APINENE and BPINENE chemistry in CRI-Strat.

Tropospheric CO in the StratTrop mechanism was evaluated against multiple datasets by Archibald et al. (2020). They found significant negative biases in column CO of 10-20 DU over much of the Northern hemisphere, but similar values across the Southern
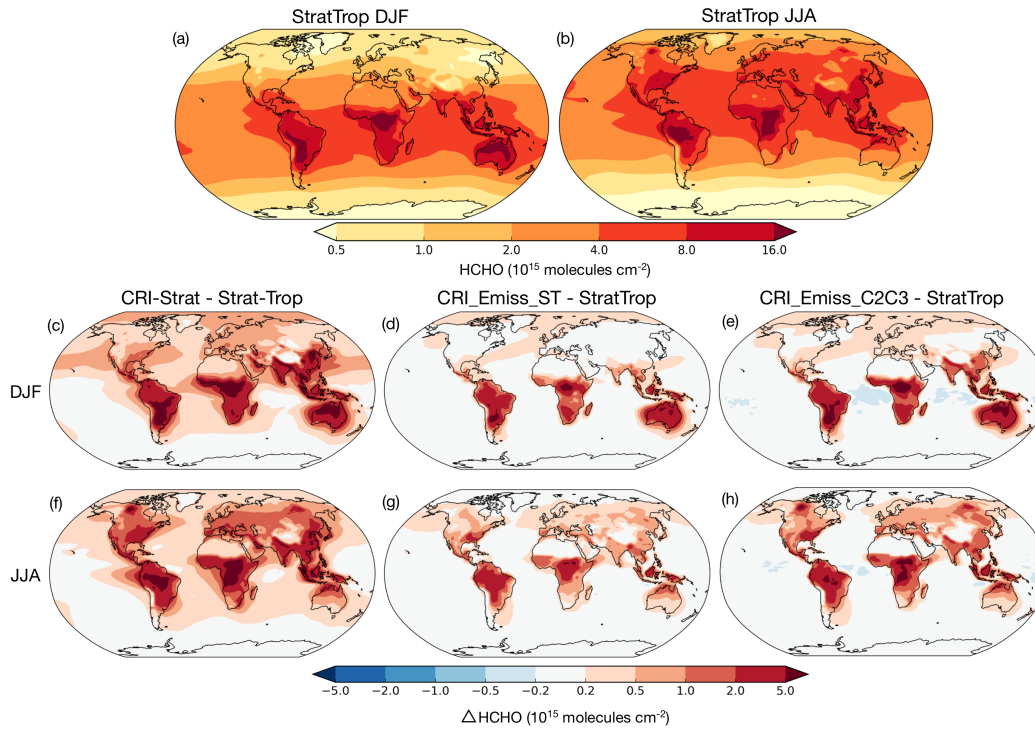
Figure 11. Average tropospheric column HCHO in StratTrop simulations for DJF (a) and JJA (b). Differences in tropospheric HCHO column density in DJF and JJA between CRI-Strat and StratTrop (c, f), CRI_Emiss_ST and StratTrop (d, g), and CRI_Emiss_C2C3 and StratTrop (e, h).

hemisphere and a high bias over BVOC rich Central Africa and Amazonia compared to the MOPITT satellite product. The CRI-Strat simulation has a lot more CO in the Northern hemisphere, reducing the negative bias there, but far too much CO in the southern hemisphere particularly downwind of BVOC sources. Although the CRI-Strat mechanism captures secondary production of CO better than StratTrop, it highlights that too much CO production occurs in the southern hemisphere, likely due to errors in BVOC emissions. In addition, the model setup either lacks some key CO or CO precursor emissions in the Northern hemisphere, CO lifetime is too short in the model and/or not enough CO is being transported from low to high latitudes.

This importance of HCHO in CO production is emphasised in Figure 11, which shows much higher HCHO column densities above high BVOC emission regions in all of the simulations that use CRI-Strat chemistry. As HCHO is the dominant source of secondary CO, this will lead to higher CO burdens downwind. The more explicit representation of isoprene and monoterpene degradation chemistry clearly leads to greater secondary production of HCHO and as a result CO.

5.5 Peroxy Radicals

Peroxy radicals (RO_2) are formed from the oxidation of VOCs and are important but short-lived intermediates in tropospheric ozone formation. The largest differences between the two chemical mechanisms centre around treatment of RO_2 species, as discussed in section 3.1. The CRI-Strat has a total of 47 RO_2 species (as opposed to 9 in StratTrop), all of which undergo reactions with NO, NO_3, HO_2 and the summed RO_2

Table 7. Overview of average tropospheric CO burden and key fluxes for CO production/loss and for peroxy radical reactions

Flux		CRI-Strat	StratTrop	CRI_Emiss_ST	CRI_Emiss_C2C3
CO burden (Tg)		354.9	300.2	317.2	315.2
CO lifetime (days)		39.1	38.6	38.1	37.2
CO production	**Total**	**3402**	**2915**	**3121**	**3171**
(Tg CO year^{-1})	Emissions	1111 (32.7%)	1111 (38.1%)	1111 (35.6%)	1111 (35%)
	HCHO + OH	580.3 (17.1%)	492 (16.9%)	551 (17.7%)	566 (17.8%)
	HCHO + $h\nu$	1293 (38%)	1076 (36.9%)	1163 (37.3%)	1177 (37.1%)
	Other Chem	125 (3.7%)	71.5 (2.5%)	101 (3.25%)	107 (3.4%)
	Other Phot	293 (8.6%)	164 (5.6%)	194 (6.23%)	211 (6.7%)
CO Loss	**Total**	**3311**	**2841**	**3041**	**3090**
(Tg CO year^{-1})	CO + OH	3157 (95.4%)	2704 (95.2%)	2900 (95.4%)	2948 (95.4%)
	CO Dry Dep	153 (4.6%)	137 (4.8%)	141 (4.7%)	142 (4.6%)
RO$_2$ fluxes	**Total**	**111.5**	**75.8**	**91.5**	**87.9**
(P mole year^{-1})	RO$_2$ + NO	18.4 (16.5%)	11.4 (15.0%)	14.1 (15.4%)	13.1 (14.9%)
	RC(O)O$_2$ + NO$_2$ (PAN Prod)	20.6 (18.5%)	19.6 (25.9%)	14.7 (16.1%)	14.0 (16.0%)
	RO$_2$ + NO$_3$	0.3 (0.3%)	0.2 (0.3%)	0.3 (0.3%)	0.2 (0.3%)
	RO$_2$ + HO$_2$	60.4 (54.2%)	41.2 (54.4%)	52.4 (57.3%)	51.0 (58.0%)
	RO$_2$ + RO$_2$	11.8 (10.6%)	3.4 (4.5%)	10.1 (11.04%)	9.5 (10.8%)

radical pool in ways that conserve the number of potential ozone forming steps. Acetyl peroxy radicals ($RC(O)O_2$) are also crucial as they form thermally stable peroxyacetyl nitrate (PAN) compounds, important NO_y reservoir species. CRI-Strat has multiple addition PAN species from degradation of higher NMVOC species. Table 7 gives a summary of the key RO_2 reaction fluxes in the troposphere. The CRI-Strat simulation has a 50% higher RO_2 flux compared to StratTrop. The CRI_Emiss_ST and CRI_Emiss_C2C3 simulations have total fluxes 20% and 16% higher than StratTrop respectively, showing that a large fraction of the additional flux is a result of the more explicit multigeneration chemistry, and not just from the additional NMVOC emissions in CRI-Strat.

There are big differences in the respective fates of RO_2 species. In the CRI-Strat mechanism, RO_2 species are more than twice as likely to react with another RO_2 species than in StratTrop, because the full range of these cross-reactions are parameterised for all RO_2 species. The CRI-Strat mechanisms also have a greater flux through the $RO_2 + HO_2$ branches, which form ROOH species which are then often lost via wet and dry deposition, due to higher HO_2 and RO_2 concentrations in CRI-Strat (see Table 6). There is a much larger flux through PAN forming reactions in StratTrop. The MPAN forming reaction in StratTrop is much faster than the equivalent reaction in CRI-Strat (see supplementary Figure S5), and hence the production of MPAN and PAN-type species is greater in StratTrop even though all other PAN-type species (including PAN) are formed in greater abundance in CRI-Strat. However, as PAN-type species rapidly dissociate back to the original reactants in high temperature conditions, the higher flux through the $RC(O)O_2 + NO_2$ pathway does not necessarily lead to permanent oxidation, unlike via the other branches.

5.6 Nitrogen Oxides and their reservoirs

There are stark differences in nitrogen oxides between the different model simulations, as shown in Figure 12. In this analysis, we use the StratTrop simulation as a baseline to evaluate CRI-Strat, as StratTrop in UKESM1 has been thoroughly evaluated by Archibald et al. (2020). In the StratTrop simulation, the tropospheric column density of NO_2 is highest over polluted regions, such as China and Europe, and is higher in local winter than summer, due to higher emissions, and lower oxidising capacity and photolysis rates in winter (Fig. 12 (a, b)). Archibald et al. (2020) found a high bias downwind of these polluted regions in winter of up to 5×10^{15} molecules cm^{-2} (approximately 50%) compared to the OMI satellite product, but a small low bias over most of the rest of the world (see Archibald et al. (2020) Fig. 18). The CRI-Strat simulation has much lower column density of NO_2 across the Northern Hemisphere continental regions in winter such as over China where CRI-Strat has column densities more than 5×10^{15} molecules cm^{-2} lower than StratTrop (Fig. 12 (c)). CRI_Emiss_ST has lower NO_2 column than StratTrop directly over high emission regions but is similar downwind (Fig. 12 (d, g)). CRI_Emiss_C2C3 is somewhere between the base CRI-Strat and CRI_Emiss_ST simulations, with a lower column density of NO_2 over polluted regions and downwind of them over continents, but not to the same degree as CRI-Strat (Fig. 12 (e, h)).

Nitrogen is conserved through chemical reactions (noting that some minor changes were made to the StratTrop mechanism in order for it to conserve nitrogen, see Section S3 in the supplement for details) and all simulations have exactly the same NO_x emissions, therefore if NO_2 is lower it must have been converted into some other form and/or lost via deposition. It is conventional to use the shorthand NO_x as the sum of nitrogen oxides NO and NO_2, NO_z is the sum of their reservoir species, and NO_y is the sum of all oxidised nitrogen compounds:

$$NO_x = NO + NO_2 \tag{9}$$

$$NO_z = HONO_2 + NO_3 + 2*N_2O_5 + HO_2NO_2 + XONO_2 + PANs + RONO_2 + CH_3O_2NO_2 + Nitrophenols \tag{10}$$

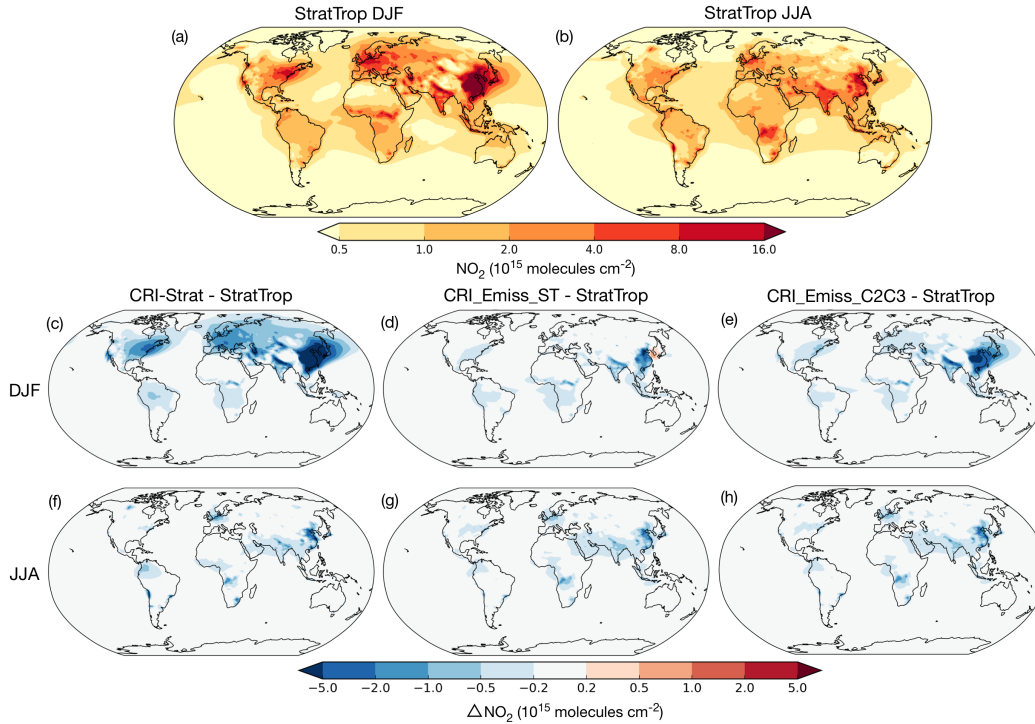$$NO_y = NO_x + NO_z \tag{11}$$

Figure 12. Average tropospheric column NO_2 in StratTrop simulations for DJF (a) and JJA (b). Differences in tropospheric NO_2 column in DJF and JJA between CRI-Strat and StratTrop (c, f), CRI_Emiss_ST and StratTrop (d, g), and CRI_Emiss_C2C3 and StratTrop (e, h).

The conversion of NO_x to NO_z can inhibit the ozone forming process. The most component of NO_z is nitric acid ($HONO_2$), which is efficiently dry and wet deposited and so acts as a sink for reactive nitrogen in the troposphere. However, some reservoir species (such as PAN) can also aid overall ozone production if they are transported, releasing NO_x into other regions of the troposphere where the ozone forming potential per NO_x molecule is greater.

When analysing how oxidised nitrogen differs between these model simulations, its important to understand some key differences between the two chemical mechanisms. The CRI-Strat mechanism has the same inorganic nitrogen species as StratTrop, but it has many more organic nitrogen containing species which contribute to NO_z. Firstly, in CRI-Strat almost every $RO_2 + NO$ reaction has a minor branch which forms an organonitrate ($RONO_2$), whereas in StratTrop only CH_3ONO_2 and ISON (which represents organonitrates from isoprene oxidation) exist. Peroxy radicals with nitrate groups are also formed from NO_3 initiated reactions with alkenes, which can also go on to form stable organonitrates. These organonitrates can act as NO_x reservoirs, transported long distances before undergoing further oxidation or photolysis to release NO_x or getting deposited out of the atmosphere. CRI-Strat also has several more PAN-type species, formed from thermal equilibrium between peroxyacyl radicals and NO_2. Finally, there are some species in CRI-Strat for which there is no equivalent in StratTrop: $CH_3O_2NO_2$ is formed from the thermal equilibrium between CH_3O_2 and NO_2 and can be an important reservoir species in the upper troposphere (Browne et al., 2011), while nitrated phenols are formed during the oxidation of benzene and toluene in the presence of NO_x (Harrison et al., 2005).

Zonal mean differences in these summed species are shown in Figure 13. There is reduced NO_x in the CRI-Strat mechanism compared to StratTrop (Fig. 13 (a)), partic-
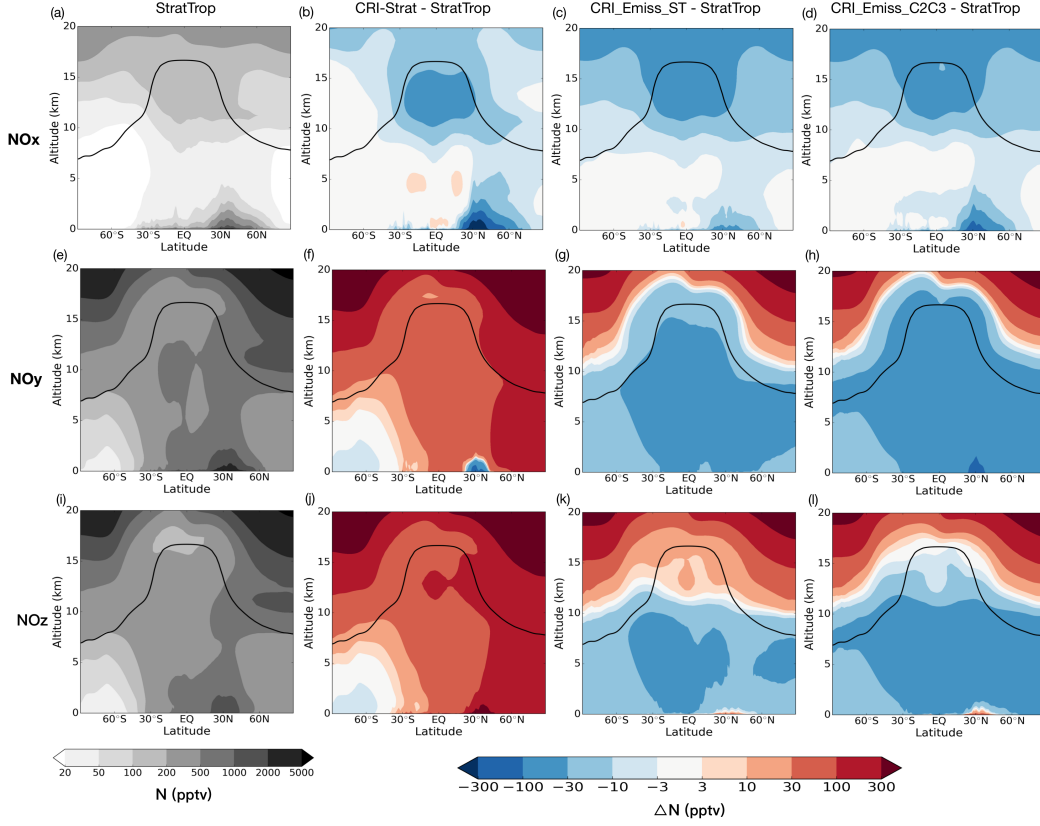
Figure 13. Average zonal mean NO_x (a), NOy (e) and NO_z (f) in StratTrop run from 2010-2018. Zonal mean differences in NO_x, NO_y and NO_z between CRI-Strat and StratTrop (b, f and j), CRI_Emiss_ST and StratTrop (c, g and k), and CRI_Emiss_C2C3 and StratTrop (d, h, l) respectively. Black lines show average tropopause height over simulation period.

ularly in the lower atmosphere in the northern hemisphere and in the upper troposphere, that is visible in the base CRI-Strat simulation (Fig. 13 (b)) and in the runs with same total NMVOC mass emissions to StratTrop (Fig. 13 (c and d)). In contrast, total oxidised nitrogen NO_y is generally higher in CRI-Strat compared to StratTrop (Fig. 13 (e and f)), except in the lower atmosphere around 30°N (specifically over East Asia and India, see supplementary Figure S13), but lower almost everywhere in CRI_Emiss_ST and CRI_Emiss_C2C3 (Fig. 13 (g and h)). The increase in NO_y is shown to be due to there being more NO_z almost everywhere in the CRI-Strat model simulation compared to StratTrop (Fig. 13 (j)). However, in the CRI-STEmiss and CRI_Emiss_C2C3 simulations higher NO_z is only found in the lower atmosphere northern hemisphere downwind of high emitting regions (Fig. 13 (k and l)). Hence the increased NO_z in the CRI-Strat simulation is clearly tied in with the extra NMVOC emissions. Without these added organic species, the CRI-Strat chemical mechanism has greater propensity to produce more NO_z in polluted regions but loose oxidised nitrogen mass overall.

The base CRI-Strat simulation has more tropospheric NO_y than StratTrop (1.112 Tg N vs. 1.018 Tg N), but has less of the total nitrogen as NO_x (10.3% vs 14.9%) and more as NO_z reservoirs (89.7% vs 85.1%), as shown in Table 8. However, CRI-Strat has a smaller fraction of NO_y as $HONO_2$ (45.8% vs 50.4%), the single largest component of NO_z. Instead, a greater fraction is stored as PANs and $RONO_2$, as well as $CH_3O_2NO_2$ and nitrophenol species which are not in the StratTrop chemical mechanism.

Table 8. Overview of tropospheric oxidised nitrogen burdens (fraction of total NO_y in brackets), tropospheric oxidised nitrogen emission and deposition fluxes, stratosphere-troposphere transfer (STT) and NO_y lifetime in the troposphere (fraction of total NO_y deposition in brackets).

	CRI-Strat	StratTrop	CRI.Emiss.ST	CRI.Emiss.C2C3
NO_y Burden (Tg N)	1.112	1.018	0.950	0.910
NO_x Burden (Tg N)	0.115 (10.3%)	0.152 (14.9%)	0.136 (14.3%)	0.131 (14.4%)
NO_z Burden (Tg N)	0.998 (89.7%)	0.866 (85.1%)	0.814 (85.7%)	0.779 (85.6%)
$HONO_2$ Burden (Tg N)	0.509 (45.8%)	0.513 (50.4%)	0.506 (53.2%)	0.512 (56.2%)
Other inorganic NO_z (Tg N)	0.021 (1.9%)	0.018 (1.7%)	0.018 (1.9%)	0.019 (2.1%)
PANs (Tg N)	0.367 (33.0%)	0.296 (29.1%)	0.245 (25.8%)	0.206 (22.7%)
$RONO_2$ (Tg N)	0.061 (5.5%)	0.039 (3.9%)	0.038 (4.0%)	0.035 (3.9%)
$CH_3O_2NO_2$ (Tg N)	0.008 (0.7%)	N/A	0.007 (0.7%)	0.007 (0.7%)
Nitrophenols (Tg N)	0.031 (2.8%)	N/A	0.0	0.0
Total NO_x Emissions (Tg N year^{-1})	61.5	61.5	61.5	61.5
Total NO_y Deposition (Tg N year^{-1})	63.0	62.9	63.0	63.0
Inferred STT (Tg N year^{-1})	1.46	1.40	1.43	1.44
NO_x Dry deposition (Tg N year^{-1})	6.83 (10.8%)	7.70 (12.2%)	7.36 (11.7%)	7.25 (11.5%)
$HONO_2$ Wet deposition (Tg N year^{-1})	29.0 (46.0%)	30.1 (47.8%)	30.1 (47.8%)	30.0 (47.7%)
$HONO_2$ Dry deposition (Tg N year^{-1})	22.0 (34.9%)	21.6 (34.3%)	22.3 (35.5%)	22.4 (35.6%)
Other inorganic NO_z deposition (Tg N year^{-1})	1.21 (1.9%)	0.97 (1.6%)	1.04 (1.6%)	1.08 (1.7%)
PANs dry deposition (Tg N year^{-1})	1.70 (2.7%)	1.28 (2.0%)	0.894 (1.4%)	0.918 (1.5%)
$RONO_2$ deposition (Tg N year^{-1})	2.09 (3.3%)	1.30 (2.1%)	1.22 (2.0%)	1.28 (2.0%)
Nitrophenol deposition (Tg N year^{-1})	0.22 (0.4%)	N/A	0.0	0.0
NO_y deposition lifetime (days)	6.44	5.91	5.51	5.28
$HONO_2$ deposition lifetime (days)	3.65	3.62	3.53	3.57
PANs deposition lifetime (days)	78.9	84.5	100.1	82.0
$RONO_2$ deposition lifetime (days)	10.7	11.0	11.4	9.99

Many of these differences can be attributed to the added NMVOC emissions in the CRI-Strat simulations. The greater total quantity of NMVOC emissions, added larger NMVOCs and the explicit depiction of their multigenerational degradation provides more opportunities for NO_z reservoir species to form. In the CRI_Emiss_ST simulation, the total tropospheric NO_y is 0.95 Tg N, showing that the CRI-Strat mechanism has lower NO_y when if run with the same NMVOC emissions as StratTrop (Table 8). The fraction of NO_x (14.3%) is slightly lower than StratTrop, but still higher than CRI-Strat. In the CRI_Emiss_C2C3 simulation, NO_y is lower still, at 0.91 Tg N. The driving factor behind these differences appears to be a greater fraction of total NO_y as $HONO_2$ in CRI_Emiss_ST (53.2%) and CRI_Emiss_C2C3 (56.2%) compared to StratTrop (50.4%) or the base CRI-Strat run (45.8%). However, CRI_Emiss_ST and CRI_Emiss_C2C3 both have slightly less $HONO_2$ than StratTrop in absolute terms.

The importance of these differences in oxidised nitrogen species burdens can be better understood by analysing the sources and sinks of oxidised nitrogen in the troposphere. In all of the simulations, total NO_x emissions are identical, and total NO_y deposition almost identical, as shown in Table 8. Total NO_y deposition is greater than total emissions because of net transfer of NO_y species (mostly $HONO_2$) from the stratosphere to the troposphere, with this additional NO_y originating from reaction of N_2O and $O(^1D)$ in the stratosphere. From the tropospheric NO_y burden and sum of all deposition sinks, we can calculate the mean tropospheric NO_y lifetime, which ranges from around 6.4 days in CRI-Strat to 5.9 days in StratTrop, 5.5 days in CRI_Emiss_ST and only 5.3 days in CRI_Emiss_C2C3. By decomposing the channels by which NO_y is deposited, we can see that less is deposited as NO_x or $HONO_2$ in CRI-Strat compared to StratTrop, and a larger fraction is deposited as organic nitrogen containing species. In general these organic nitrogen-containing species deposit less efficiently than $HONO_2$ (R. Sander, 2015) and have longer lifetimes with respect to deposition, effectively extending the NO_y lifetime and allowing total NO_z to accumulate (Table 8). They are also more effective at transporting NO_x from polluted regions and releasing it in cleaner regions which are more NO_x sensitive, going a long way to explaining why the CRI-Strat simulation has the highest overall rate of ozone production (Table 5).

Compared to the StratTrop model run, the CRI_Emiss_ST and CRI_Emiss_C2C3 simulations have similar wet deposition loss of $HONO_2$ but greater loss via dry deposition. This is because there is more $HONO_2$ production in the boundary layer (see supplementary Figure S14), where it can be rapidly lost via dry deposition before it has time to be transported away from emission sources. Hence, total tropospheric NO_z and NO_y levels, and NO_y lifetime, are overall lower in CRI_Emiss_ST and CRI_Emiss_C2C3 compared to StratTrop.

5.7 Summary and synthesis

Collating all of the information covered in this analysis, we can understand that the variations in tropospheric ozone are largely driven by the variations in the NO_y fields between the simulations:

1. In polluted regions, ozone production is more efficient in the CRI-Strat mechanism due to the more explicit representation of multigenerational NMVOC-NOx chemistry, particularly when the amount of NMVOC available is increased. However, loss of ozone is also more rapid, particularly due to the increased proportion of O_x lost via the $O(^1D) + H_2O$ reaction.

2. The enhanced $HONO_2$ production in CRI-Strat leads to greater NO_y removal in the boundary layer via dry deposition, reducing the amount entering the free troposphere.

3. In the base CRI-Strat run, faster $HONO_2$ production is compensated by greater production of organic nitrogen-containing species which extend the lifetime of NO_y and enhance ozone production in remote regions.

4. These competing effects roughly balance over the whole troposphere, leading to similar tropospheric ozone burdens in the CRI-Strat and StratTrop simulations, albeit with more ozone near the surface in CRI-Strat.

5. The CRI_Emiss_ST and CRI_Emiss_C2C3 simulations are less able to form organonitrates than the CRI-Strat simulation so lose more nitrogen to $HONO_2$ deposition and therefore have lower NO_y burdens. Combined with the shorter ozone lifetime, these two simulations have the lowest tropospheric ozone burdens despite having higher ozone production rates than StratTrop in the polluted boundary layer.

Overall, we find a strong sensitivity between emissions of NMVOCs and the oxidised nitrogen budget, which leads to considerable knock on effects to the tropospheric ozone burden and oxidising capacity of the atmosphere. This has important implications for the need to improve emissions of NMVOCs (which are typically poorly constrained (Huang et al., 2017)) and how these emissions are treated in simpler mechanisms such as StratTrop. The dependence of NO_x to emissions of NMVOCs is also relevant for how we interpret comparisons of NO_x between models and observations.

The CRI mechanism has now been implemented in a number of models, including STOCHEM (S. Utembe et al., 2010) and WRF-Chem (Archer-Nicholls et al., 2014). The STOCHEM implementation also saw an increase in ozone production and loss compared to its existing mechanism, but this led to much higher ozone burdens across the troposphere, particularly over the oceans. In contrast, CRI-Strat has similar tropospheric ozone burdens to StratTrop and lower ozone concentrations across much of the world's oceans. We believe the higher tropospheric ozone columns did not occur in UKCA because of the shorter O_x lifetime in CRI-Strat compared to StratTrop due to the faster flux through the $O(^1D) + H_2O$ reaction in CRI-Strat. The WRF-Chem implementation also saw an increase in ozone production but little overall increase in ozone over the model domain compared to the CBM-Z mechanism. However, in a regional model a species such as ozone, with a typical lifetime of a few weeks, is very sensitive to the effects of boundary conditions. In Archer-Nicholls et al. (2014), boundary conditions were prescribed by the MOZART model for both CBM-Z and CRIv2-R5. Combining WRF-Chem with boundary conditions driven by UKCA simulations, with both models using the same CRI mechanism, could offer a solution to the problem of how to account for the impact of boundary conditions.

6 Conclusions

The CRIv2-R5 chemical mechanism has been integrated into the UKCA model, merged with the existing stratospheric chemistry and coupled to GLOMAP-mode aerosol to create the CRI-Strat mechanism. The mechanism is constrained to reliably reproduce the ozone forming potential from MCMv3.1, enabling traceability to our best understanding and providing a benchmark to evaluate simpler mechanisms and test other aspects of model setup. This new mechanism marks a step change in chemical complexity and comprehensiveness, improving representation of important tropospheric processes, such as BVOC chemistry, peroxy radicals and organonitrates, while remaining sufficiently affordable for use in an Earth System Model (approximately 75% longer runtime compared to an equivalent run with StratTrop). CRI-Strat can now be used in UKESM1, a flagship model used for CMIP6 (Eyring et al., 2016), opening up new potential scientific enquiries. As the implementation has been done using the ASAD framework (Carver et al., 1997), it can also be ported to other models which share the same framework.

In this paper we critically evaluate and compare CRI-Strat to the well-established StratTrop mechanism, highlighting some key differences:

1. CRI-Strat has higher surface ozone and CO compared to StratTrop, improving some biases compared to observations but worsening others.
2. CRI-Strat chemistry is generally "hotter" than StratTrop: it has much higher production and loss of ozone, more HO_x and more secondary production of CO.
3. Total tropospheric ozone burden and ozone column density are surprisingly similar between the simulations, given the large differences in production rate.
4. CRI-Strat partitions a greater fraction of nitrogen into reservoir forms (NO_z) with a lower fraction in the reactive form (NO_x).
5. Many differences are related to the speciation of NMVOCs. Significantly more emitted species are included in CRI-Strat than in StratTrop. When using exactly the same emissions, CRI-Strat has 8.6% lower tropospheric ozone burden than StratTrop.

Some of these differences reflect differences in reaction rate coefficients for key reactions, a number of which are out of date in CRIv2-R5 and therefore CRI-Strat. The faster production of ozone that occurs in CRI-Strat when photochemical conditions allow means that it is more sensitive to model structural uncertainties than StratTrop, particularly relating to emissions, model resolution and parameterisations such as for lightning-NO_x emissions. The more complex CRI-Strat mechanism is not designed to be a replacement for StratTrop, but provides a new tool that expands the possible scientific questions that can be tackled with the model and a benchmark to evaluate against.

The tests and evaluation described in this paper set out to fully characterise the CRI-Strat mechanism against the StratTrop mechanism (the reference mechanism for UEKSM1) for the gas-phase composition of species relevant for the climate. This provides information that is essential to understand and make use of the new mechanism. However, the experiments performed do not use CRI-Strat to its full potential. We expect it to exceed the capabilities of StratTrop when run at higher spatial resolution and in evaluation against field campaigns with a focus on oxidants. Future work will also focus on highly polluted environments or those dominated by BVOCs and production of SOA, for which CRI has been shown to provide a robust framework for simulating (S. Utembe et al., 2010). We also plan to run experiments for different climate and emission regimes such as the pre-industrial atmosphere; these experiments (combined with multi model analyses) will enable us to understand if we can be confident that UKESM1 represents the changes in composition and chemistry-climate feedbacks from pre-industrial to the present day realistically. This evaluation has also neglected analysis of aerosols, whose formation rates will differ with CRI-Strat due to changes in oxidant fields, and will be properly evaluated in the future. There is also scope to improve the coupling between CRI-Strat and the GLOMAP-mode scheme, for example updating reaction rates and extending the isoprene chemistry with inclusion of CRIv2.2 (M. E. Jenkin, Khan, et al., 2019), improving representation of BVOC environments, OH recycling and further expansion with HOM chemistry (Weber et al., 2020).

Acknowledgments

sions of atmospheric Compounds and Compilation of Ancillary Data (ECCAD) archive. We would also like to thank the Tropospheric Ozone Assessment Report (TOAR) initiative for providing access to the aggregated surface ozone statistics that they have calculated using data collected from multiple stations and networks globally. Development and application of the OMI ozone profile retrieval scheme was funded through NERC-NCEO and ESA Climate Change Initiative. The authors declare no conflicts of interest.

Due to intellectual property right restrictions, we cannot provide either the source code or documentation papers for the UM. The Met Office Unified Model is available for use under licence. The functionality described here is fully available in the UM trunk from version 11.8. A number of research organisations and national meteorological services use the UM in collaboration with the UK Met Office to undertake basic atmospheric process research, produce forecasts, develop the UM code and build and evaluate Earth system models. For further information on how to apply for a licence; see `https://www.metoffice.gov.uk/research/approach/modelling-systems/unified-model` (last access: 24 November 2020). Data tables of the full CRI-Strat mechanism as described in this paper are included in the supplement.

UM simulations are compiled and run in suites developed using the Rose suite engine (`http://metomi.github.io/rose/doc/html/index.html`, last access: 24 November 2020) and scheduled using the Cylc workflow engine (`https://cylc.github.io/`, last access: 24 November 2020). Both Rose and Cylc are available under version 3 of the GNU General Public License (GPL). In this framework, the suite contains the information required to extract and build the code as well as configure and run the simulations. Each suite is labelled with a unique identifier and is held in the same revision-controlled repository service in which we hold and develop the model's code. This means that these suites are available to any licensed user of the UM. The input emissions data are available from Input4MIPs (`https://esgf-node.llnl.gov/projects/input4mips/`, last access: 24 November 2020).

References

Akimoto, H. (2003, dec). Global air quality and pollution. *Science (New York, N.Y.)*, *302*(5651), 1716–9. Retrieved from `http://www.ncbi.nlm.nih.gov/pubmed/14657488` doi: 10.1126/science.1092666

Andreae, M. O. (1990). Ocean-atmosphere interactions in the global biogeochemical sulfur cycle. *Marine Chemistry*, *30*(C), 1–29. doi: 10.1016/0304-4203(90)90059-L

Archer-Nicholls, S., Lowe, D., Utembe, S., Allan, J., Zaveri, R. A., Fast, J. D., . . . McFiggans, G. (2014, nov). Gaseous chemistry and aerosol mechanism developments for version 3.5.1 of the online regional model, WRF-Chem. *Geoscientific Model Development*, *7*, 2557–2579. Retrieved from `http://www.geosci-model-dev.net/7/2557/2014/` doi: 10.5194/gmd-7-2557-2014

Archibald, A., O'Connor, F., Abraham, N. L., Archer-Nicholls, S., Chipperfield, M., Dalvi, M., . . . Zeng, G. (2020). Description and evaluation of the UKCA stratosphere-troposphere chemistry scheme (StratTrop vn 1.0) implemented in UKESM1. *Geoscientific Model Development*, *13*, 1223–1266. doi: 10.5194/gmd-2019-246

Atkinson, R. (1990). Gas-phase tropospheric chemistry of organic compounds: a review. *Atmospheric Environment*, *24A*(1), 1–41. Retrieved from `http://linkinghub.elsevier.com/retrieve/pii/S1352231007009934` doi: 10.1016/j.atmosenv.2007.10.068

Atkinson, R., Baulch, D. L., Cox, R. A., Crowley, J. N., Hampson, R. F., Hynes, R. G., . . . Rossi, M. J. (2004). Evaluated kinetic and photochemical data for atmospheric chemistry : Volume I – gas phase reactions of Ox, HOx, NOx and

SOx species. *Atmospheric Chemistry and Physics*, *4*, 1461–1738.

Atkinson, R., Baulch, D. L., Cox, R. A., Crowley, J. N., Hampson, R. F., Hynes, R. G., . . . Troe, J. (2006, sep). Evaluated kinetic and photochemical data for atmospheric chemistry: Volume II – gas phase reactions of organic species. *Atmospheric Chemistry and Physics*, *6*(11), 3625–4055. Retrieved from http://www.atmos-chem-phys.net/6/3625/2006/ doi: 10.5194/acp-6-3625-2006

Atkinson, R., Baulch, D. L., Cox, R. A., Hampson, R. F., Kerr, J. A., Rossi, M. J., & Troe, J. (1997). Evaluated Kinetic and Photochemical Data for Atmospheric Chemistry Supplement VI. *J. Phys. chem. Ref. Data*, *26*(6), 1329–1499.

Aumont, B., Szopa, S., & Madronich, S. (2005). Modelling the evolution of organic carbon during its gas-phase tropospheric oxidation: Development of an explicit model based on a self generating approach. *Atmospheric Chemistry and Physics*, *5*(9), 2497–2517. doi: 10.5194/acp-5-2497-2005

Banerjee, A., Archibald, A. T., Maycock, A. C., Telford, P., Abraham, N. L., Yang, X., . . . Pyle, J. A. (2014). Lightning NOx, a key chemistry-climate interaction: Impacts of future climate change and consequences for tropospheric oxidising capacity. *Atmospheric Chemistry and Physics*, *14*(18), 9871–9881. doi: 10.5194/acp-14-9871-2014

Bates, K. H., & Jacob, D. J. (2020). An Expanded Definition of the Odd Oxygen Family for Tropospheric Ozone Budgets: Implications for Ozone Lifetime and Stratospheric Influence. *Geophysical Research Letters*, *47*(4), 1–9. doi: 10.1029/2019GL084486

Bianchi, F., Kurtén, T., Riva, M., Mohr, C., Rissanen, M. P., Roldin, P., . . . Ehn, M. (2019). Highly Oxygenated Organic Molecules (HOM) from Gas-Phase Autoxidation Involving Peroxy Radicals: A Key Contributor to Atmospheric Aerosol. *Chemical Reviews*. doi: 10.1021/acs.chemrev.8b00395

Boersma, K. F., Eskes, H. J., Veefkind, J. P., Brinksma, E. J., Van Der A, R. J., Sneep, M., . . . Bucsela, E. J. (2007). Atmospheric Chemistry and Physics Near-real time retrieval of tropospheric \chem{NO_2} from OMI. *Atmos. Chem. Phys*, *7*, 2103–2118. Retrieved from www.atmos-chem-phys.net/7/2103/2007/

Boucher, O., Randall, D., Artaxo, P., Bretherton, C., Feingold, G., Forster, P., . . . Zhang, X. (2013). Clouds and Aerosols. In T. Stocker et al. (Eds.), *Climate change 2013: The physical science basis. contribution of working group i to the fifth assessment report of the intergovernmental panel on climate change.* Cambridge, United Kingdom and New York, NY, USA: Cambridge University Press.

Bowman, K. W., Shindell, D. T., Worden, H. M., Lamarque, J. F., Young, P. J., Stevenson, D. S., . . . Worden, J. R. (2013). Evaluation of ACCMIP outgoing longwave radiation from tropospheric ozone using TES satellite observations. *Atmospheric Chemistry and Physics*, *13*(8), 4057–4072. doi: 10.5194/acp-13-4057-2013

Browne, E. C., Perring, A. E., Wooldridge, P. J., Apel, E., Hall, S. R., Huey, L. G., . . . Cohen, R. C. (2011). Global and regional effects of the photochemistry of CH3O2NO2: Evidence from ARCTAS. *Atmospheric Chemistry and Physics*, *11*(9), 4209–4219. doi: 10.5194/acp-11-4209-2011

Carver, G., Brown, P., & Wild, O. (1997). The ASAD atmospheric chemistry integration package and chemical reaction database. *Computer Physics Communications*, *105*(2), 197–215. doi: 10.1016/S0010-4655(97)00056-8

Chipperfield, M. P. (2006). New version of the TOMCAT/SLIMCAT off-line chemical transport model: Intercomparison of stratospheric tracer experiments. *Quarterly Journal of the Royal Meteorological Society*, *132*(617), 1179–1203. doi: 10.1256/qj.05.51

Collins, W. J., Lamarque, J.-F., Schulz, M., Boucher, O., Eyring, V., Hegglin, M. I.,

... Smith, S. J. (2017). AerChemMIP: Quantifying the effects of chemistry and aerosols in CMIP6. *Geoscientific Model Development*, *10*, 585–607. Retrieved from http://www.geosci-model-dev-discuss.net/gmd-2016-139/ doi: 10.5194/gmd-2016-139

Dee, D. P., Uppala, S. M., Simmons, A. J., Berrisford, P., Poli, P., Kobayashi, S., ... Vitart, F. (2011). The ERA-Interim reanalysis: Configuration and performance of the data assimilation system. *Quarterly Journal of the Royal Meteorological Society*, *137*(656), 553–597. doi: 10.1002/qj.828

Derwent, R. (2017). Intercomparison of chemical mechanisms for air quality policy formulation and assessment under North American conditions. *Journal of the Air & Waste Management Association*, *00*(00), 10962247.2017.1292969. Retrieved from https://www.tandfonline.com/doi/full/10.1080/10962247.2017.1292969 doi: 10.1080/10962247.2017.1292969

Dobber, M. R., Dirksen, R. J., Levelt, P. F., Van Den Oord, G. H., Voors, R. H., Kleipool, Q., ... Rozemeijer, N. C. (2006). Ozone monitoring instrument calibration. *IEEE Transactions on Geoscience and Remote Sensing*, *44*(5), 1209–1238. doi: 10.1109/TGRS.2006.869987

Esenturk, E., Abraham, L., Archer-Nicholls, S., Mitsakou, C., Griffiths, P., & Pyle, J. (2018). Quasi-Newton Methods for Atmospheric Chemistry Simulations : Implementation in UKCA UM Vn10 . 8. *Geoscientific Model Development*, *11*, 1–31. doi: 10.5194/gmd-2018-32

Eyring, V., Bony, S., Meehl, G. A., Senior, C. A., Stevens, B., Stouffer, R. J., & Taylor, K. E. (2016). Overview of the Coupled Model Intercomparison Project Phase 6 (CMIP6) experimental design and organization. *Geoscientific Model Development*, *9*(5), 1937–1958. doi: 10.5194/gmd-9-1937-2016

Fenech, S., Doherty, R. M., Heaviside, C., Vardoulakis, S., Macintyre, H. L., & O'Connor, F. M. (2018). The influence of model spatial resolution on simulated ozone and fine particulate matter for Europe: Implications for health impact assessments. *Atmospheric Chemistry and Physics*, *18*(8), 5765–5784. doi: 10.5194/acp-18-5765-2018

Feng, L., Smith, S. J., Braun, C., Crippa, M., Gidden, M. J., & Hoesly, R. (2020). The generation of gridded emissions data for CMIP6. *Geoscientific Model Development*, *13*, 461–482.

Gaudel, A., Cooper, O. R., Ancellet, G., Barret, B., Boynard, A., Burrows, J. P., ... Lewis, A. (2018). Tropospheric Ozone Assessment Report: Present-day distribution and trends of tropospheric ozone relevant to climate and global atmospheric chemistry model evaluation. *Elem Sci Anth*, *6*. doi: 10.1525/elementa.291

Giannakopoulos, C., Chipperfield, M. P., Law, K. S., & Pyle, J. A. (1999). Validation and Intercomparison of Wet and Dry Model Deposition Schemes Using 210Pb in a Global Three-Dimensional off-line Chemical Transport Model. *Journal of Geophysical Research*, *104*(D19), 23,761–23,784.

Goldstein, A. H., & Galbally, I. E. (2007). Known and unexplored organic constituents in the earth's atmosphere. *Environmental Science and Technology*, *41*(5), 1514–1521. doi: 10.1021/es072476p

Grant, A., Archibald, A. T., Cooke, M. C., & Shallcross, D. E. (2010). Modelling the oxidation of seventeen volatile organic compounds to track yields of CO and CO2. *Atmospheric Environment*, *44*(31), 3797–3804. Retrieved from http://dx.doi.org/10.1016/j.atmosenv.2010.06.049 doi: 10.1016/j.atmosenv.2010.06.049

Guenther, A. B., Jiang, X., Heald, C. L., Sakulyanontvittaya, T., Duhl, T., Emmons, L. K., & Wang, X. (2012, nov). The Model of Emissions of Gases and Aerosols from Nature version 2.1 (MEGAN2.1): an extended and updated framework for modeling biogenic emissions. *Geoscientific Model Development*, *5*, 1471–1492. Retrieved from http://www.geosci-model-dev.net/5/1471/

2012/ doi: 10.5194/gmd-5-1471-2012

Harrison, M. A., Barra, S., Borghesi, D., Vione, D., Arsene, C., & Iulian Olariu, R. (2005). Nitrated phenols in the atmosphere: A review. *Atmospheric Environment*, *39*(2), 231–248. doi: 10.1016/j.atmosenv.2004.09.044

Hayman, G. D. (1997). Effects of Pollution Control on UV Exposure, AEA Technology Final Report. *prepared for the Department of Health on Contract 121/6377, AEA Technology*, *Reference AEA/RCEC/22522001/R/002 ISSUE1*.

Heald, C. L., & Kroll, J. H. (2020). The fuel of atmospheric chemistry: Toward a complete description of reactive organic carbon. *Science Advances*, *6*(6), 1–9. doi: 10.1126/sciadv.aay8967

Hodzic, A., Campuzano-Jost, P., Bian, H., Chin, M., Colarco, P. R., Day, D. A., ... Jimenez, J. L. (2020). Characterization of organic aerosol across the global remote troposphere: A comparison of ATom measurements and global chemistry models. *Atmospheric Chemistry and Physics*, *20*(8), 4607–4635. doi: 10.5194/acp-20-4607-2020

Hoerling, M. P., Schaack, T. K., & Lenzen, A. J. (1993). A Global Analysis of Stratospheric-Tropospheric Exchange during Northern Winter. *Monthly Weather Review*, *121*(1), 162–172.

Hoesly, R. M., Smith, S. J., Feng, L., Klimont, Z., Janssens-Maenhout, G., Pitkanen, T., ... Zhang, Q. (2018). Historical (1750-2014) anthropogenic emissions of reactive gases and aerosols from the Community Emissions Data System (CEDS). *Geoscientific Model Development*, *11*(1), 369–408. doi: 10.5194/gmd-11-369-2018

Hood, C., MacKenzie, I., Stocker, J., Johnson, K., Carruthers, D., Vieno, M., & Doherty, R. (2018). Air quality simulations for London using a coupled regional-to-localmodelling system. *Atmospheric Chemistry and Physics*, *18*, 11221–11245. doi: 10.5194/acp-2017-1202

Hoyle, C. R., Marécal, V., Russo, M. R., Allen, G., Arteta, J., Chemel, C., ... Zeng, G. (2011). Representation of tropical deep convection in atmospheric models - Part 2: Tracer transport. *Atmospheric Chemistry and Physics*, *11*(15), 8103–8131. doi: 10.5194/acp-11-8103-2011

Huang, G., Brook, R., Crippa, M., Janssens-Maenhout, G., Schieberle, C., Dore, C., ... Friedrich, R. (2017). Speciation of anthropogenic emissions of non-methane volatile organic compounds: A global gridded data set for 1970-2012. *Atmospheric Chemistry and Physics*, *17*(12), 7683–7701. doi: 10.5194/acp-17-7683-2017

Jenkin, M., & Clemitshaw, K. (2000). Ozone and other secondary photochemical pollutants: chemical processes governing their formation in the planetary boundary layer. *Atmospheric Environment*, *34*(16), 2499–2527. Retrieved from http://linkinghub.elsevier.com/retrieve/pii/S1352231099004781 doi: 10.1016/S1352-2310(99)00478-1

Jenkin, M., Saunders, S. M., & Pilling, M. J. (1997, jan). The tropospheric degradation of volatile organic compounds: a protocol for mechanism development. *Atmospheric Environment*, *31*(1), 81–104. Retrieved from http://linkinghub.elsevier.com/retrieve/pii/S1352231096001057 doi: 10.1016/S1352-2310(96)00105-7

Jenkin, M., Watson, L., Utembe, S., & Shallcross, D. (2008, oct). A Common Representative Intermediates (CRI) mechanism for VOC degradation. Part 1: Gas phase mechanism development. *Atmospheric Environment*, *42*, 7185–7195. Retrieved from http://linkinghub.elsevier.com/retrieve/pii/S1352231008006742 doi: 10.1016/j.atmosenv.2008.07.028

Jenkin, M. E., Khan, M. A., Shallcross, D. E., Bergström, R., Simpson, D., Murphy, K. L., & Rickard, A. R. (2019). The CRI v2.2 reduced degradation scheme for isoprene. *Atmospheric Environment*, *212*(May), 172–182. doi:

10.1016/j.atmosenv.2019.05.055

Jenkin, M. E., Saunders, S. M., Derwent, R. G., & Pilling, M. J.   (2002, oct).   Development of a reduced speciated VOC degradation mechanism for use in ozone models. *Atmospheric Environment*, *36*(30), 4725–4734. Retrieved from `http://linkinghub.elsevier.com/retrieve/pii/S1352231002005630`   doi: 10.1016/S1352-2310(02)00563-0

Jenkin, M. E., Saunders, S. M., Wagner, V., & Pilling, M. J.   (2003, feb).   Protocol for the development of the Master Chemical Mechanism, MCM v3 (Part B): tropospheric degradation of aromatic volatile organic compounds.   *Atmospheric Chemistry and Physics*, *3*(1), 181–193.   Retrieved from `http://www.atmos-chem-phys.net/3/181/2003/`   doi: 10.5194/acp-3-181-2003

Jenkin, M. E., Valorso, R., Aumont, B., & Rickard, A. R.   (2019).   Estimation of rate coefficients and branching ratios for reactions of organic peroxy radicals for use in automated mechanism construction.   *Atmospheric Chemistry and Physics*(19), 7691–7717. doi: 10.5194/acp-2019-44

Jenkin, M. E., Valorso, R., Aumont, B., Rickard, A. R., & Wallington, T. J. (2018a). *Estimation of rate coefficients and branching ratios for gas-phase reactions of OH with aliphatic organic compounds for use in automated mechanism construction* (Vol. 18) (No. 13). doi: 10.5194/acp-18-9297-2018

Jenkin, M. E., Valorso, R., Aumont, B., Rickard, A. R., & Wallington, T. J.   (2018b).   Estimation of rate coefficients and branching ratios for gas-phase reactions of OH with aromatic organic compounds for use in automated mechanism construction.   *Atmospheric Chemistry and Physics*, *18*(13), 9329–9349. doi: 10.5194/acp-18-9329-2018

Jenkin, M. E., Wyche, K. P., Evans, C. J., Carr, T., Monks, P. S., Alfarra, M. R., . . . Rickard, A. R. (2012). Development and chamber evaluation of the MCM v3.2 degradation scheme for β-caryophyllene.   *Atmospheric Chemistry and Physics*, *12*(11), 5275–5308. doi: 10.5194/acp-12-5275-2012

Jenkin, M. E., Young, J. C., & Rickard, A. R.   (2015).   The MCM v3.3.1 degradation scheme for isoprene. *Atmospheric Chemistry and Physics*, *15*(20), 11433–11459. doi: 10.5194/acp-15-11433-2015

Jimenez, J. L., Canagaratna, M. R., Donahue, N. M., Prevot, a. S. H., Zhang, Q., Kroll, J. H., . . . Worsnop, D. R.   (2009, dec).   Evolution of organic aerosols in the atmosphere.   *Science (New York, N.Y.)*, *326*(5959), 1525–9. Retrieved from `http://www.ncbi.nlm.nih.gov/pubmed/20007897`   doi: 10.1126/science.1180353

Khan, M. A., Clements, J., Lowe, D., McFiggans, G., Percival, C. J., & Shallcross, D. E.   (2019).   Investigating the behaviour of the CRI-MECH gas-phase chemistry scheme on a regional scale for different seasons using the WRF-Chem model.   *Atmospheric Research*, *229*(June), 145–156.   Retrieved from `https://doi.org/10.1016/j.atmosres.2019.06.021`   doi: 10.1016/j.atmosres.2019.06.021

Khan, M. A. H., Cooke, M. C., Utembe, S. R., Archibald, A. T., Derwent, R. G., Xiao, P., . . . Shallcross, D. E.   (2015).   Global modeling of the nitrate radical (NO3) for present and pre-industrial scenarios.   *Atmospheric Research*, *164-165*(3), 347–357. doi: 10.1016/j.atmosres.2015.06.006

Lightfoot, P. D., Cox, R. A., Crowley, J. N., Destriau, M., Hayman, G. D., Jenkin, M. E., . . . Zabel, F.   (1992).   Organic peroxy radicals: kinetics, spectroscopy and tropospheric chemistry. *Atmospheric Environment*, *26*(10), 1805–1961.

Lowe, D., Archer-Nicholls, S., Morgan, W., Allan, J., Utembe, S., Ouyang, B., . . . McFiggans, G.   (2015).   WRF-chem model predictions of the regional impacts of N2O5 heterogeneous processes on nighttime chemistry over north-western Europe.   *Atmospheric Chemistry and Physics*, *15*, 1385–1409.   Retrieved from `http://www.atmos-chem-phys-discuss.net/14/20883/2014/`   doi: 10.5194/acp-15-1385-2015

Mann, G. W., Carslaw, K. S., Spracklen, D. V., Ridley, D. A., Manktelow, P. T., & Chipperfield, M. P. (2010). Description and evaluation of GLOMAP-mode : a modal global aerosol microphysics model for the UKCA composition-climate model. *Geoscientific Model Development*, 519–551. doi: 10.5194/gmd-3-519-2010

Mcfiggans, G., Mentel, T. F., Wildt, J., Pullinen, I., Kang, S., Kleist, E., . . . Kiendler-scharr, A. (2019). Secondary organic aerosol reduced by mixture of atmospheric vapours. *Nature*, 0–6. Retrieved from http://dx.doi.org/10.1038/s41586-018-0871-y doi: 10.1038/s41586-018-0871-y

McGillen, M. R., Carter, W. P., Mellouki, A., J. Orlando, J., Picquet-Varrault, B., & J. Wallington, T. (2020). Database for the kinetics of the gas-phase atmospheric reactions of organic compounds. *Earth System Science Data*, *12*(2), 1203–1216. doi: 10.5194/essd-12-1203-2020

Monks, P. S. (2005, may). Gas-phase radical chemistry in the troposphere. *Chemical Society reviews*, *34*(5), 376–95. Retrieved from http://www.ncbi.nlm.nih.gov/pubmed/15852151 doi: 10.1039/b307982c

Monks, P. S., Archibald, A. T., Colette, A., Cooper, O., Coyle, M., Derwent, R., . . . Williams, M. L. (2015). Tropospheric ozone and its precursors from the urban to the global scale from air quality to short-lived climate forcer. *Atmospheric Chemistry and Physics*, *15*(15), 8889–8973. doi: 10.5194/acp-15-8889-2015

Morgenstern, O., Braesicke, P., O'Connor, F. M., Bushell, A. C., Johnson, C. E., Osprey, S. M., & Pyle, J. A. (2009). Evaluation of the new UKCA climate-composition model – Part 1: The stratosphere. *Geoscientific Model Development*, *2*, 43–57. Retrieved from http://www.geosci-model-dev.net/2/43/2009/gmd-2-43-2009.html doi: 10.5194/gmd-2-43-2009

Mulcahy, J. P., Johnson, C., Jones, C., Povey, A., Sellar, A., Scott, C. E., . . . Yool, A. (2020). Description and evaluation of aerosol in UKESM1 and HadGEM3-GC3.1 CMIP6 historical simulations. *Geoscientific Model Development*.

Mulcahy, J. P., Jones, C., Sellar, A., Johnson, B., Boutle, I. A., Jones, A., . . . Mc-Coy, D. T. (2018). Improved Aerosol Processes and Effective Radiative Forcing in HadGEM3 and UKESM1. *Journal of Advances in Modeling Earth Systems*, *10*(11), 2786–2805. doi: 10.1029/2018MS001464

Neu, J. L., Prather, M. J., & Penner, J. E. (2007). Global atmospheric chemistry: Integrating over fractional cloud cover. *Journal of Geophysical Research Atmospheres*, *112*(11), 1–12. doi: 10.1029/2006JD008007

Newsome, B., & Evans, M. (2017). Impact of uncertainties in inorganic chemical rate constants on tropospheric composition and ozone radiative forcing. *Atmospheric Chemistry and Physics*, *17*(23), 14333–14352. doi: 10.5194/acp-17-14333-2017

Novelli, A., Kaminski, M., Rolletter, M., Acir, I. H., Bohn, B., Dorn, H. P., . . . Fuchs, H. (2018). Evaluation of OH and \chem{HO_2} concentrations and their budgets during photooxidation of 2-methyl-3-butene-2-ol (MBO) in the atmospheric simulation chamber SAPHIR. *Atmospheric Chemistry and Physics*, *18*(15), 11409–11422. doi: 10.5194/acp-18-11409-2018

O'Connor, F. M., Johnson, C. E., Morgenstern, O., Abraham, N. L., Braesicke, P., Dalvi, M., . . . Pyle, J. A. (2014). Evaluation of the new UKCA climate-composition model-Part 2: The troposphere. *Geoscientific Model Development*, *7*(1), 41–91. doi: 10.5194/gmd-7-41-2014

Olivier, J. G. J., Peters, J., Granier, C., Petron, G., Muller, J.-F., & Wallens, S. (2003). Present and future surface emissions of atmospheric compounds. *POET Report #3, EU project EVK2-1999-00011*.

Orlando, J. J., & Tyndall, G. S. (2012). Laboratory studies of organic peroxy radical chemistry: An overview with emphasis on recent issues of atmospheric significance. *Chemical Society Reviews*, *41*(19), 6294–6317. doi: 10.1039/c2cs35166h

Pétron, G., Granier, C., Khattatov, B., Lamarque, J. F., Yudin, V., Müller, J. F., & Gille, J. (2002). Inverse modeling of carbon monoxide surface emissions using Climate Monitoring and Diagnostics Laboratory network observations. *Journal of Geophysical Research Atmospheres*, *107*(24), 1–23. doi: 10.1029/2001JD001305

Porter, W. C., Safieddine, S. A., & Heald, C. L. (2017). Impact of aromatics and monoterpenes on simulated tropospheric ozone and total OH reactivity. *Atmospheric Environment*, *169*, 250–257. doi: 10.1016/j.atmosenv.2017.08.048

Sander, R. (2015). Compilation of Henry's law constants (version 4.0) for water as solvent. *Atmospheric Chemistry and Physics*, *15*, 4399–4981. doi: 10.5194/acp-15-4399-2015

Sander, S. P., Friedl, R. R., Barker, J. R., Golden, D. M., Kurylo, M. J., Sciences, G. E., ... Orkin, V. L. (2011). Chemical Kinetics and Photochemical Data for Use in Atmospheric Studies Evaluation Number 17 NASA Panel for Data Evaluation :. (17).

Saunders, S. M., Jenkin, M. E., Derwent, R. G., & Pilling, M. J. (2003, feb). Protocol for the development of the Master Chemical Mechanism, MCM v3 (Part A): tropospheric degradation of non-aromatic volatile organic compounds. *Atmospheric Chemistry and Physics*, *3*, 161–180. doi: 10.5194/acp-3-161-2003

Schultz, M. G., Schröder, S., Lyapina, O., Cooper, O. R., Galbally, I., Petropavlovskikh, I., ... Zhiqiang, M. (2017). Tropospheric Ozone Assessment Report: Database and metrics data of global surface ozone observations. *Elementa*, *5*. doi: 10.1525/elementa.244

Sellar, A. A., Jones, C. G., Mulcahy, J., Tang, Y., Yool, A., Wiltshire, A., ... Zerroukat, M. (2019). UKESM1: Description and evaluation of the UK Earth System Model. *Journal of Advances in Modeling Earth Systems*. doi: 10.1029/2019ms001739

Sillman, S. (1999, jun). The relation between ozone, NOx and hydrocarbons in urban and polluted rural environments. *Atmospheric Environment*, *33*(12), 1821–1845. Retrieved from http://linkinghub.elsevier.com/retrieve/pii/S1352231098003458 doi: 10.1016/S1352-2310(98)00345-8

Sindelarova, K., Granier, C., Bouarar, I., Guenther, A., Tilmes, S., Stavrakou, T., ... Knorr, W. (2014). Global data set of biogenic VOC emissions calculated by the MEGAN model over the last 30 years. *Atmospheric Chemistry and Physics*, *14*(17), 9317–9341. doi: 10.5194/acp-14-9317-2014

Spracklen, D. V., Carslaw, K. S., Kulmala, M., Kerminen, V. M., Mann, G. W., & Sihto, S. L. (2006). The contribution of boundary layer nucleation events to total particle concentrations on regional and global scales. *Atmospheric Chemistry and Physics*, *6*(12), 5631–5648. doi: 10.5194/acp-6-5631-2006

Stock, Z. S., Russo, M. R., & Pyle, J. A. (2014). Representing ozone extremes in European megacities: The importance of resolution in a global chemistry climate model. *Atmospheric Chemistry and Physics*, *14*(8), 3899–3912. doi: 10.5194/acp-14-3899-2014

Stockwell, W. R., Middleton, P., & Chang, J. S. (1990). The Second Generation Regional Acid Deposition Model Chemical Mechanism for Regional Air Quality Modeling The most important in the gas Alkanes with between. *Journal of Geophysical Research*, *95*(D10), 16,343–16,367.

Telford, P. J., Abraham, N. L., Archibald, A. T., Braesicke, P., Dalvi, M., Morgenstern, O., ... Pyle, J. A. (2013). Implementation of the Fast-JX Photolysis scheme into the UKCA component of the MetUM chemistry climate model. *Geoscientific Model Development*, *6*, 161–177. doi: 10.5194/gmdd-5-3217-2012

Telford, P. J., Braesicke, P., Morgenstern, O., & Pyle, J. A. (2008). Technical note: Description and assessment of a nudged version of the new dynamics Unified Model. *Atmospheric Chemistry and Physics*, *8*(6), 1701–1712. doi:

10.5194/acp-8-1701-2008

Tsigaridis, K., Daskalakis, N., Kanakidou, M., Adams, P. J., Artaxo, P., Bahadur, R., ... Zhang, X. (2014). The AeroCom evaluation and intercomparison of organic aerosol in global models. *Atmospheric Chemistry and Physics*, *14*(19), 10845–10895. doi: 10.5194/acp-14-10845-2014

Tunved, P., Ström, J., & Hansson, H.-C. (2004). An investigation of processes controlling the evolution of the boundary layer aerosol size distribution properties at the Swedish background station Aspvreten. *Atmospheric Chemistry and Physics Discussions*, *4*(4), 4507–4543. doi: 10.5194/acpd-4-4507-2004

Tyndall, G. S., Cox, R. A., Granier, C., Lesclaux, R., Moortgat, G. K., Pilling, M. J., ... Wallington, T. J. (2001). Atmospheric chemistry of small organic peroxy radicals. *Journal of Geophysical Research*, *106*(D11), 12157–12182.

Utembe, S., Cooke, M., Archibald, A. T., Jenkin, M., Derwent, R., & Shallcross, D. (2010, apr). Using a reduced Common Representative Intermediates (CRIv2-R5) mechanism to simulate tropospheric ozone in a 3-D Lagrangian chemistry transport model. *Atmospheric Environment*, *44*(13), 1609–1622. Retrieved from http://linkinghub.elsevier.com/retrieve/pii/S1352231010001056 doi: 10.1016/j.atmosenv.2010.01.044

Utembe, S. R., Watson, L. A., Shallcross, D. E., & Jenkin, M. E. (2009, apr). A Common Representative Intermediates (CRI) mechanism for VOC degradation. Part 3: Development of a secondary organic aerosol module. *Atmospheric Environment*, *43*(12), 1982–1990. Retrieved from http://linkinghub.elsevier.com/retrieve/pii/S1352231009000284 doi: 10.1016/j.atmosenv.2009.01.008

Van Der Werf, G. R., Randerson, J. T., Giglio, L., Van Leeuwen, T. T., Chen, Y., Rogers, B. M., ... Kasibhatla, P. S. (2017). Global fire emissions estimates during 1997-2016. *Earth System Science Data*, *9*(2), 697–720. doi: 10.5194/essd-9-697-2017

Van Marle, M. J., Kloster, S., Magi, B. I., Marlon, J. R., Daniau, A. L., Field, R. D., ... Van Der Werf, G. R. (2017). Historic global biomass burning emissions for CMIP6 (BB4CMIP) based on merging satellite observations with proxies and fire models (1750-2015). *Geoscientific Model Development*, *10*(9), 3329–3357. doi: 10.5194/gmd-10-3329-2017

Von Schneidemesser, E., Monks, P. S., Allan, J. D., Bruhwiler, L., Forster, P., Fowler, D., ... Sutton, M. A. (2015). Chemistry and the Linkages between Air Quality and Climate Change. *Chemical Reviews*, *115*(10), 3856–3897. doi: 10.1021/acs.chemrev.5b00089

von Clarmann, T., & Glatthor, N. (2019). The application of mean averaging kernels to mean trace gas distributions. *Atmospheric Measurement Techniques Discussions*, 1–11. doi: 10.5194/amt-2019-61

von Glasow, R., & Crutzen, P. J. (2004, apr). Model study of multiphase DMS oxidation with a focus on halogens. *Atmospheric Chemistry and Physics*, *4*(3), 589–608. Retrieved from http://www.atmos-chem-phys.net/4/589/2004/ doi: 10.5194/acp-4-589-2004

Walters, D., Baran, A. J., Boutle, I., Brooks, M., Earnshaw, P., Edwards, J., ... Zerroukat, M. (2019). The Met Office Unified Model Global Atmosphere 7.0/7.1 and JULES Global Land 7.0 configurations. *Geoscientific Model Development*, *12*(5), 1909–1963. doi: 10.5194/gmd-12-1909-2019

Wang, Y., Jacob, D. J., & Logan, J. A. (1998). Global simulation of tropospheric O3-NOx-hydrocarbon chemistry - 3. Origin of tropospheric ozone and effects of nonmethane hydrocarbons. *Journal of Geophysical Research: Atmospheres*, *103*(3339), 10757–10767. doi: 10.1029/98jd00156

Waters, J. W., Froidevaux, L., Harwood, R. S., Jarnot, R. F., Pickett, H. M., Read, W. G., ... Walch, M. J. (2006). The Earth Observing System Microwave Limb Sounder (EOS MLS) on the aura satellite. *IEEE Transactions on Geoscience*

and Remote Sensing, *44*(5), 1075–1092. doi: 10.1109/TGRS.2006.873771

Watson, L., Shallcross, D., Utembe, S., & Jenkin, M. (2008, oct). A Common Representative Intermediates (CRI) mechanism for VOC degradation. Part 2: Gas phase mechanism reduction. *Atmospheric Environment*, *42*(31), 7196–7204. Retrieved from http://linkinghub.elsevier.com/retrieve/pii/S1352231008006845 doi: 10.1016/j.atmosenv.2008.07.034

Weber, J., Archibald, A., Griffiths, P., Archer-Nicholls, S., Berndt, T., Jenkin, M., ... Knote, C. (2020). CRI-HOM: A novel chemical mechanism for simulating Highly Oxygenated Organic Molecules (HOMs) in global chemistry-aerosol-climate models. *Atmospheric Chemistry and Physics*, *20*, 1–31. doi: 10.5194/acp-2020-154

Wesley, M. L. (1989). Parameterization of Surface Resistances to Gaseous Dry Deposition in Regional-Scale Numerical Models. *Atmospheric Environment*, *23*(6), 1293–1304. doi: 10.1016/S0950-351X(05)80241-1

Wild, O., & Prather, M. J. (2000). Excitation of the primary tropospheric chemical mode in a global three-dimensional model. *Journal of Geophysical Research*, *105*(D20), 24647. Retrieved from http://doi.wiley.com/10.1029/2000JD900399 doi: 10.1029/2000JD900399

Wild, O., & Prather, M. J. (2006). Global tropospheric ozone modeling: Quantifying errors due to grid resolution. *Journal of Geophysical Research Atmospheres*, *111*(11), 1–14. doi: 10.1029/2005JD006605

Wild, O., Zhu, X. I. N., & Prather, M. J. (2000). Fast-J: Accurate Simulation of In- and Below-Cloud Photolysis in Tropospheric Chemical Models. *Journal of Atmospheric Chemistry*, *37*, 245–282.

Woodward, S. (2001). Modeling the atmospheric life cycle and radiative impact of mineral dust in the Hadley Centre climate model. *Journal of Geophysical Research*, *106*(D16), 18,155–18,166.

Young, P. J., Archibald, A. T., Bowman, K. W., Lamaraque, J.-F., Stevenson, D. S., Tilmes, S., ... Zeng, G. (2013). Pre-industrial to end 21st century projections of tropospheric ozone from the Atmospheric Atmospheric Chemistry and Climate Model Intercomparison Project (ACCMIP). *Atmospheric Chemistry and Physics*, *13*(13), 2063–2090. doi: 10.5194/acp-13-5277-2013

Young, P. J., Naik, V., Fiore, A. M., Gaudel, A., Guo, J., Lin, M. Y., ... Zeng, G. (2018). Tropospheric Ozone Assessment Report: Assessment of global-scale model performance for global and regional ozone distributions, variability, and trends. *Elem Sci Anth*, *6*(1), 10. Retrieved from http://www.elementascience.org/article/10.1525/elementa.265/ doi: 10.1525/elementa.265

Zhang, K., Wan, H., Liu, X., Ghan, S. J., Kooperman, G. J., Ma, P. L., ... Lohmann, U. (2014). Technical note: On the use of nudging for aerosol-climate model intercomparison studies. *Atmospheric Chemistry and Physics*, *14*(16), 8631–8645. doi: 10.5194/acp-14-8631-2014

Ziemke, J. R., Chandra, S., Duncan, B. N., Froidevaux, L., Bhartia, P. K., Levelt, P. F., & Waters, J. W. (2006). Tropospheric ozone determined from Aura OMI and MLS: Evaluation of measurements and comparison with the Global Modeling Initiative's Chemical Transport Model. *Journal of Geophysical Research Atmospheres*, *111*(19), 1–18. doi: 10.1029/2006JD007089

Ziemke, J. R., Oman, L. D., Strode, S. A., Douglass, A. R., Olsen, M. A., McPeters, R. D., ... Taylor, S. L. (2019). Trends in Global Tropospheric Ozone Inferred from a Composite Record of TOMS/OMI/MLS/OMPS Satellite Measurements and the MERRA-2 GMI Simulation. *Atmospheric Chemistry and Physics*, *19*, 3257–3269. doi: 10.5194/acp-2018-716